The Astrophysical Journal, 830:88 (25pp), 2016 October 20 doi:10.3847/0004-637X/830/2/88


# THE TEMPERATURE EFFECT IN SECONDARY COSMIC RAYS (MUONS) OBSERVED AT THE GROUND: ANALYSIS OF THE GLOBAL MUON DETECTOR NETWORK DATA

R. R. S. de Mendonça[1], C. R. Braga[1], E. Echer[1], A. Dal Lago[1], K. Munakata[2], T. Kuwabara[3], M. Kozai[8], C. Kato[2], M. Rockenbach[1], N. J. Schuch[1], H. K. Al Jassar[4], M. M. Sharma[4], M. Tokumaru[5], M. L. Duldig[6], J. E. Humble[6], P. Evenson[7], and I. Sabbah[9]

[1] Space Geophysics Division, National Institute for Space Research, São José dos Campos, SP, 12227-010, Brazil
[2] Physics Department, Shinshu University, Matsumoto, Nagano, 390-8621, Japan
[3] Graduate School of Science, Chiba University, Chiba City, Chiba 263-8522, Japan
[4] Physics Department, Kuwait University, Kuwait City, 13060, Kuwait
[5] Solar Terrestrial Environment Laboratory, Nagoya University, Nagoya, Aichi, 464-8601, Japan
[6] School of Physical Sciences, University of Tasmania, Hobart, Tasmania, 7001, Australia
[7] Bartol Research Institute, Department of Physics and Astronomy, University of Delaware, Newark, DE 19716, USA
[8] Institute of Space and Astronautical Science, Japan Aerospace Exploration Agency (ISAS/JAXA), Sagamihara, Kanagawa 252-5210, Japan
[9] Department of Natural Sciences, College of Health Sciences, Public Authority for Applied Education and Training, Kuwait City, 72853, Kuwait
*Received 2016 March 21; revised 2016 July 11; accepted 2016 July 24; published 2016 October 14*

## ABSTRACT

The analysis of cosmic ray intensity variation seen by muon detectors at Earth's surface can help us to understand astrophysical, solar, interplanetary and geomagnetic phenomena. However, before comparing cosmic ray intensity variations with extraterrestrial phenomena, it is necessary to take into account atmospheric effects such as the temperature effect. In this work, we analyzed this effect on the Global Muon Detector Network (GMDN), which is composed of four ground-based detectors, two in the northern hemisphere and two in the southern hemisphere. In general, we found a higher temperature influence on detectors located in the northern hemisphere. Besides that, we noticed that the seasonal temperature variation observed at the ground and at the altitude of maximum muon production are in antiphase for all GMDN locations (low-latitude regions). In this way, contrary to what is expected in high-latitude regions, the ground muon intensity decrease occurring during summertime would be related to both parts of the temperature effect (the negative and the positive). We analyzed several methods to describe the temperature effect on cosmic ray intensity. We found that the mass weighted method is the one that best reproduces the seasonal cosmic ray variation observed by the GMDN detectors and allows the highest correlation with long-term variation of the cosmic ray intensity seen by neutron monitors.

*Key words:* atmospheric effects – cosmic rays – solar–terrestrial relations – Sun: general

## 1. INTRODUCTION

Cosmic rays are mainly positively charged particles (mostly protons) with high energy that travel through space without a known origin. Analysis of cosmic ray intensity variations at Earth's surface can help us to understand cosmic ray physics itself and other phenomena related to solar, interplanetary, geomagnetic and atmospheric physics (Kudela et al. 2000; Miroshnichenko 2001; Bieber et al. 2009; Dorman 2009; Heber et al. 2013).

There are many types of cosmic ray detectors. The most commonly used are neutron monitors and muon detectors. Both indirectly monitor cosmic ray particles moving in space close to Earth. As their names imply, they observe neutrons and muons generated in the process called cosmic ray cascade. When a cosmic ray particle moves toward the Earth, most of the time it interacts with atmospheric atoms/molecules, generating secondary particles such as those mentioned above, whose intensity variation with time can be influenced by atmospheric phenomena (Grieder 2001; Dorman 2004). The atmospheric pressure changes are the main atmospheric effect on the cosmic ray intensity observed by these instruments. In short, the pressure (or barometric) influence consists of changes of absorption, decay and generation effects on secondary cosmic rays at the atmosphere that produces a time variation of its intensity anti-correlated to atmospheric pressure fluctuations. See Sagisaka (1986) or Dorman (2004) for more details. Generally, this effect is clearly observed when low- or high-pressure atmospheric systems pass through the detector's field of view and it is described and corrected through a barometric coefficient, which gives the cosmic ray intensity variation (in percent) per unit of atmospheric pressure change.

In addition to the pressure influence, temperature changes produce significant intensity variations in the case of muon detectors. The temperature effect influences the creation and disintegration processes of muons in the atmosphere. Generally, the temperature effect is described in two parts: positive and negative. The positive effect is related to the temperature influence on pion decay, which is the major source of muons in the cosmic ray cascade process. The higher the temperature, the lower the atmospheric pion absorption, which implies a higher generation rate of muons (Duperier 1951). In its turn, the negative effect is associated with changes of the muon average path along the atmosphere. It is expected that most muons are generated at higher altitude in summer due to the atmosphere expansion occurring during this period. Thus, they have a longer path to cross before reaching the ground, which allows more of them to decay, causing a decrease in their intensity at surface (Blackett 1938). Considering that low-energy muons have a higher probability to decay, a small change in their path related to the temperature effect can be easily noticed when we are monitoring their intensity at ground. On the other hand, small modifications in the path of high-energy muons are not simple to observe due their lower decay probability. In a simple approximation of the temperature effect theory described by Sagisaka (1986), the positive effect

($\alpha_p$) for a given zenith angle is inversely proportional to the integral muon intensity ($I$) and directly proportional to the product between the muon survival probability ($W$) and the temperature influence ($D_T$) on the muon production spectrum ($\Phi$), i.e., $\alpha_p \propto I^{-1} \cdot W \cdot D_T[\Phi]$. On the other hand, the negative effect ($\alpha_n$) is directly proportional to the temperature influence on the muon survival probability multiplied by the muon production spectrum, i.e., $\alpha_n \propto I^{-1} \cdot D_T[\mathrm{W}] \cdot \Phi$. As $W$ is lower for low-energy muons, a small temperature variation can produce significant changes in this parameter. In contrast, a strong temperature variation is necessary to generate a significant modification in the survival probability of high-energy muons, which has a high value. An opposite situation occurs when considering the rate of muon production by pion decay. A small temperature variation produces a more noticeable change in this parameter for high-energy muons, which has a lower initial value (non-influenced by temperature) when compared to low-energy muons. In this way, it is expected that the positive effect is dominant ($\alpha_p \gg \alpha_n$) for high-energy muons, while the negative effect predominates for low-energy muons.

It has been long known that the main effect of the temperature influence on ground muon detectors is a seasonal variation in their data, which presents a harmonic behavior with maximum value during wintertime (Hess 1940).

Temperature variations also affect the cosmic ray intensity observed by the neutron monitors, but less significantly than in the case of muon detectors. The origin of this temperature effect is related to the fact that some of the neutrons generated in the cosmic ray shower are coming from pion/muon components (Harman & Hatton 1968; Dorman 2004; Bieber et al. 2009).

Atmospheric pressure and temperature variations are linked phenomena. However, their effects on cosmic ray intensity are generally treated separately due to the complexity of analyzing both at the same time. There are many methods of analyzing and removing the temperature effect from cosmic ray intensity observed by ground muon detectors. The simplest methods consist of the comparison of the cosmic ray intensity with: surface temperature changes, the variation of the altitude of maximum muon production (MMP), or the temperature variation at this altitude (Blackett 1938; Hess 1940; Duperier 1949; Trefall 1955a; French & Chasson 1959; Okazaki et al. 2008; De Mendonça et al. 2013). There are also methods that consider the temperature variation along the entire atmosphere through empirical or theoretical analyses (Sagisaka 1986; Dorman 2004; Berkova et al. 2011; De Mendonça et al. 2013).

In this work, we analyzed the temperature effect on the four ground muon detectors of the Global Muon Detector Network (GMDN). We used the daily mean cosmic ray intensity observed by this network between 2007 January and 2012 December combined with atmospheric temperature data of balloon and remote sensing spacecraft. We compared the results obtained using empirical and theoretical methods by analyzing which ones best reproduce the seasonal cosmic ray variation observed by each GMDN detector. We also compared the muon data corrected by temperature using each method to the average cosmic ray intensity seen by neutron monitors, which practically are not affected by the temperature effect.

## 2. THE GLOBAL MUON DETECTOR NETWORK (GMDN)

Since 1992, the GMDN has been used to study cosmic ray variations related to solar, interplanetary, and atmospheric phenomena. It has been used for studying the directional anisotropy of high-energy cosmic ray intensity which often shows a dynamic variation when an interplanetary coronal mass ejection (ICME) accompanied by a strong shock approaches and arrives at the Earth (Okazaki et al. 2008). It also has been used for studying the physical aspects of these interplanetary structures (Munakata et al. 2005; Kuwabara et al. 2009). Furthermore, the GMDN has been used for studying a specific cosmic ray flux variation called loss-cone anisotropy, often recorded prior to the arrival at the Earth of interplanetary disturbances related to solar phenomena, which can be used as a tool for space weather prediction (Kuwabara et al. 2006; Fushishita et al. 2010; Rockenbach et al. 2014). The appropriate removal of temperature effect on GMDN data may improve the results of these studies.

Currently, the GMDN is composed of four ground muon detectors located at: Nagoya—Japan (NGY, 35.15°N, 136.97° E, altitude $h$ equal to 0.077 km, geomagnetic cutoff rigidity $R_c$ equal to 11.5 GV); Kingston—Australia (HBT, 43.0°S, 147.29°E, $h = 0.065$ km, $R_c = 1.8$ GV; before 2002 it was located in Hobart, and is usually called the Hobart or HBT detector); Sao Martinho da Serra—Brazil (SMS, 29.44°S, 53.81°W, $h = 0.488$ km, $R_c = 9.3$ GV); and Kuwait City—Kuwait (KWT, 9.37°N, 47.98°E, $h = 0.019$ km, $R_c = 13.80$ GV). The first and the last two detectors are installed in a room with controlled temperature. Considering the period between 2007 January and 2012 December, the temperature in the SMS detector room was around $21 \pm 2$ °C for 60% of the time and its absolute value exceeds the average on five or more degrees only for 3% of the total period. For KWT, the room temperature presented values around $23 \pm 2$ °C for 80% of the time. Only for 5% of the period do its absolute values exceed the average by five or more degrees. The room temperature is not recorded by NGY detector electronics, but it was controlled to be $20 \pm 1$ °C throughout a year.[10]

The NGY, HBT and SMS detectors are constructed using plastic scintillators and photomultipliers. Their operation started, respectively, in 1970, 1992 and 2001. Nowadays, their detection areas are 36, 16 and 32 m$^2$. They are formed by two horizontal layers of individual counters separated vertically by 1.68 m of free space plus a 0.05 m thick lead layer between them. The cosmic ray intensity is monitored in different directions depending on which top and bottom individual detectors observe a cosmic particle in coincidence. After the installation of a new correlation system (in 2005 December for SMS, 2006 August for HBT and 2007 May for NGY), the number of directional channels available in each detector drastically increased. They changed from 17 to 121 (37 with margin of statistical count rate error $\leqslant 1\%$) for NGY, from 13 to 49 (21 with error $\leqslant 1\%$) for HBT, and from 13 to 105 (33 with error $\leqslant 1\%$) for SMS. More details about this new correlation system can been found in Yasue et al. (2003).

The KWT detector started its operation in 2006. It is a hodoscope detector composed of four horizontal layers of counter tubes of 5 m length and 10 cm diameter. Two layers have tubes aligned with the north–south (NS) direction and two layers have tubes aligned with the east–west (EW) direction. One NS and one EW layer are located in the upper part of the detector, which are vertically separated by 80 cm of the remaining NS and EW layers located in the lower part. Until

[10] http://www.stelab.nagoya-u.ac.jp/ste-www1/div3/muon/dbtext22.pdf

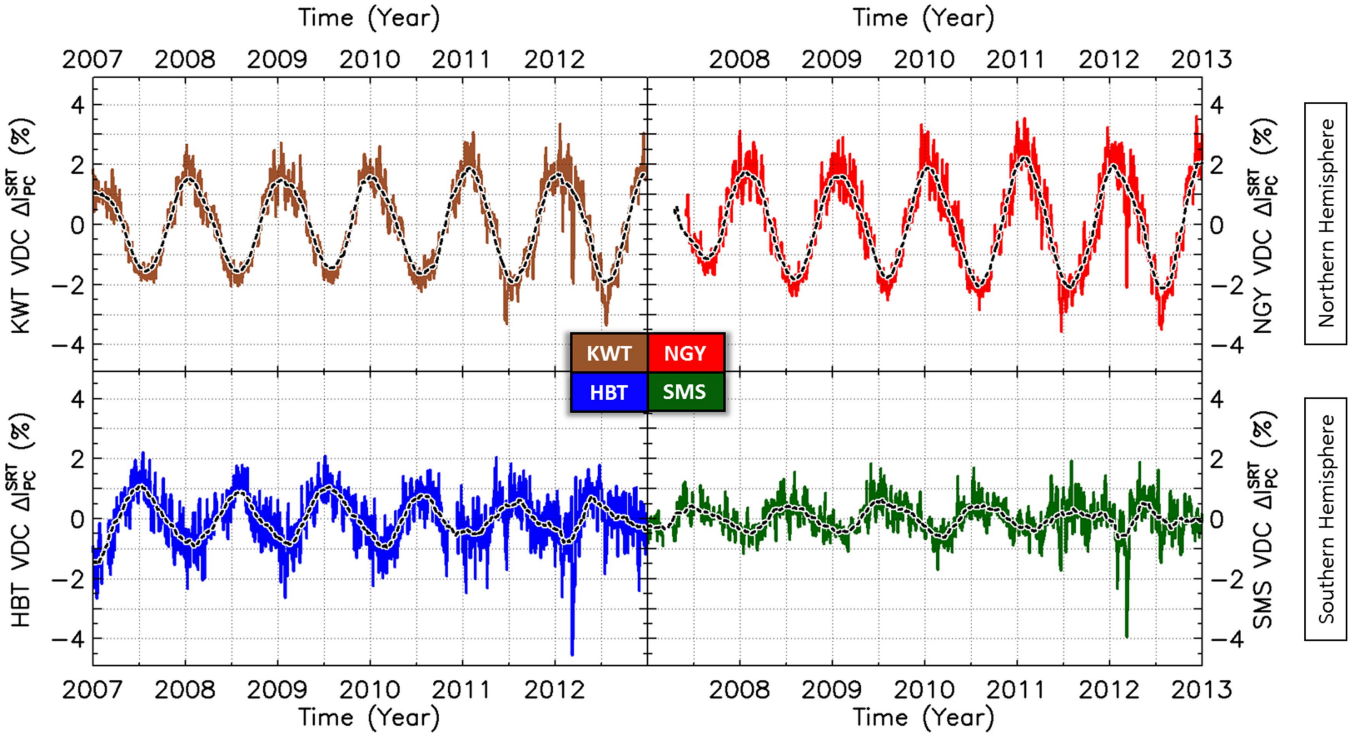


**Figure 1.** Short-term muon intensity variation corrected by pressure ($\Delta I_{PC}^{SRT}$) observed by the vertical directional channel (VDC) of the Kuwait (KWT), Nagoya (NGY), Hobart (HBT) and São Martinho da Serra (SMS) detectors from 2007 January until 2012 December. The colored curves show daily data, while black dashed curves show a 13 month running average of this data.

2015, 30 proportional counter tubes made up each layer, giving a detection area of 9 $m^2$. The combination of coincident observation by one tube of each layer allows the construction of 529 directional channels (75 with margin of statistical count rate error $\leqslant 1\%$). There is a lead blanket of 5 cm of thickness above the detector for eliminating the influence of low-energy particles.

According to the response function (which essentially gives the link between the secondary particles seen by a detector and the primary particles considering its composition and energy spectrum, the atmospheric and geomagnetic particle transport and the detection efficiency) calculated for the GMDN, taking into account the equations described by Murakami et al. (1979), we expected that all detectors presented a major response for primary cosmic rays with energies above $R_c$. While the vertical directional channel (VDC) of the new correlation system of HBT and SMS response to primary particles with median energy ($P_m$) is close to 55 GV, $P_m$ is about 59 GV for KWT and NGY. In this way, we can take into account a small effect due to $R_c$ differences on GMDN VDC muon data.

In this work, we only used pressure-corrected data recorded by the VDC of the new correlation system of each detector, which observed particles arriving at zenith angle close to zero ($<10°$ for KWT and $<30°$ for NGY, HBT, and SMS). The pressure effect on all GMDN VDC data was removed using the barometric coefficients and the methodology described by Mendonça et al. (2013) and also in the Appendix. After applying this methodology, we can see that the daily mean muon intensity variation corrected by pressure effect ($\Delta I_{PC}$) observed by the VDC of all GMDN presents a seasonal variation that can be fitted by a sinusoidal function. This seasonal variation presents maximum values during winter and minimum during summer of the hemisphere where each detector is located. Beyond this seasonal variation, $\Delta I_{PC}$ presents short- and long-term variations related to solar and interplanetary phenomena. In some analyses presented in this work, we used the short-term variation of daily muon intensity corrected by atmospheric pressure ($\Delta I_{PC}^{SRT}$) to avoid the influence of solar cycle modulation. This variable is calculated by subtracting from $\Delta I_{PC}$ a 13 month running average of itself. In Figure 1, we can see the behavior of $\Delta I_{PC}^{SRT}$ obtained for each detector. In this figure, it is possible to see that the seasonal variation amplitude of NGY and KWT is higher than that present on the muon data of HBT and SMS. Short-term solar or interplanetary influence, such as that responsible for the occurrence of Forbush decreases, is still present in $\Delta I_{PC}^{SRT}$. However, the impact of this kind of event is small over the full time period of the dataset and it should not affect the analysis of the seasonal variation and the study of the temperature effect.

## 3. TEMPERATURE DATA

We used daily atmospheric temperature profiles obtained using data collected above each GMDN site by radiosondes onboard meteorological balloons and by the SABER (Sounding of the Atmosphere using Broadband Emission Radiometry) instrument, which is on board the *TIMED* (*Thermosphere, Ionosphere, Mesosphere Energetics and Dynamics*) spacecraft.

The SABER instrument is an infrared radiometer which, among other measurements, can retrieve temperature profiles of the middle atmosphere using broadband measurements of $CO_2$ emission radiation at 15 $\mu$m (Earth limb emission). This technique has been used for many years since its development in the 1970s (Gille & House 1971). More information about this instrument can be found in Mlynczak et al. (2007) and in

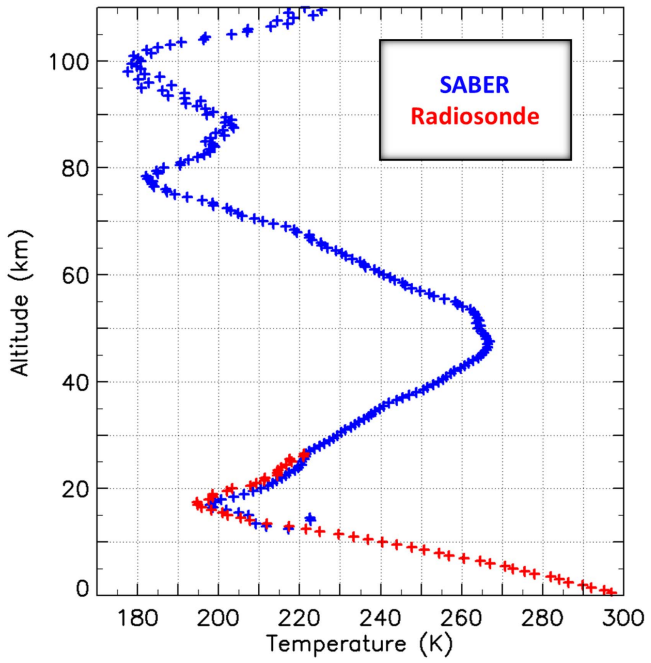


**Figure 2.** Atmospheric temperature profile composite using SABER (blue) and radiosonde (red) data observed above the SMS detector region on 2009/11/06.

its database.[11] Usually, the SABER instrument cannot measure temperature at altitudes below 14–15 km. In order to obtain temperature values in this altitude range, we used radiosonde data provided by the Integrated Global Radiosonde Archive, which is available through the NOAA/ESRL Radiosonde Database.[12] We processed SABER and radiosonde data observed between 0.5 and 110 km of altitude to obtain daily temperature values for layers with a width of 0.5 km. We can see an example of an atmospheric temperature profile obtained using SABER (red points) and radiosonde (blue points) data in Figure 2. In the altitude range where red and blue points overlap, we calculated an average value using both data sets.

Figure 3 shows the temperature deviation observed at two different altitudes above each detector location from 2007 January up to 2012 December. We show the deviations obtained on the altitude closest to the ground ($\Delta T\,[h_{\rm GRD}]$, $h_{\rm GRD} = 0.5$ km) and closest to the altitude of maximum production of secondary cosmic ray particles ($\Delta T\,[h_{\rm MMP}]$, $h_{\rm MMP} = 16.5$ km). In this figure, we can observe that $\Delta T\,[h_{\rm GRD}]$ (dark color curves) present a seasonal variation with maximum during summer, while the $\Delta T\,[h_{\rm MMP}]$ (light color curves) presents an antiphase seasonal variation, i.e., with maximum during winter.

As shown in Figure 4, we can also see this situation in temperature data allocated in fixed steps of isobaric atmospheric layers rather than altitude ranges. In this figure, we show the temperature deviation observed above each GMDN detector at the 100 hPa isobar line (where the MMP occurs). The hourly temperature data shown in this figure were processed by the IZMIRAN (Nikolay Pushkov Institute of Terrestrial Magnetism, Ionosphere and Radio Wave Propagation of the Russian Academy of Sciences) and made available on its Muon Detector Database.[13] In this database, they used data of the Global Forecast System Model[14] (GFS) and the Global Data Assimilation System[15] (GDAS) developed and supported by the NCEP (National Centers for Environmental Prediction) of the NOAA (National Oceanic and Atmospheric Administration) agency.

Considering this antiphase between the seasonal variation of atmospheric temperature observed close to the ground and close to the altitude of maximum production of secondary cosmic rays (~100 hPa), we can expect a ground muon intensity decrease during the summer related to both (positive and negative) temperature effects. Due to the negative effect, we expect a decrease in the muon intensity related to the atmospheric expansion associated with the ground temperature increase during the summer. In the same period, due to the positive effect, we also expect a ground muon intensity decrease related to the temperature decrease at the altitude of maximum secondary cosmic ray production.

However, this situation is not true for the entire globe. For the IceCube Experiment location (south pole region), the seasonal variation of the temperature observed at 100 hPa isobar line is in phase with that observed at ground (see Figure 1 of Tilav et al. 2009 or IceCube temperature data in the IZMIRAN database). This situation can also be seen in the atmospheric temperature data for Uragan muon detector location (high north latitude) provided by IZMIRAN. Moreover, analysis of atmospheric temperatures through FORMOSAT-3/COSMIC (Formosa Satellite mission-3/Constellation Observing System for Meteorology, Ionosphere, and Climate) has shown that this condition is observed for higher latitude (>40°) regions (see Figure 9 of Liu et al. 2014). Therefore, unlike what occurs in the case of GMDN (lower latitude regions), the positive and negative temperature effects have an opposite influence in the ground muon intensity observed at those locations.

## 4. METHODS FOR DESCRIBING AND REMOVING THE TEMPERATURE EFFECT

Generally, the methods for describing the temperature effect consist of a way to calculate the muon intensity variation expected due to this effect ($\Delta I_T$). Therefore, for obtaining the muon intensity variation corrected by temperature and pressure effects ($\Delta I_{\rm TPC}$), we need to subtract $\Delta I_T$ from the observed muon intensity variation corrected by pressure ($\Delta I_{\rm PC}$):

$$\Delta I_{\rm TPC} = \Delta I_{\rm PC} - \Delta I_T. \quad (1)$$

In this work, we analyze seven methods that describe the temperature effect on the muon intensity observed by ground detectors. We also analyze some variations and combinations of these methods. We now describe each of them.

### 4.1. The Atmospheric Expansion (ATE) Method

This method only considers the temperature effect related to the atmospheric expansion phenomenon taking into account the altitude variation of an atmospheric layer with a chosen isobaric pressure. In this way, we can write the muon intensity

[11] http://saber.gats-inc.com
[12] http://www.esrl.noaa.gov/raobs/General_Information.html
[13] http://cr20.izmiran.ru/MDDB/
[14] http://www.ncdc.noaa.gov/data-access/model-data/model-datasets/global-forcast-system-gfs
[15] https://www.ncdc.noaa.gov/data-access/model-data/model-datasets/global-data-assimilation-system-gdas

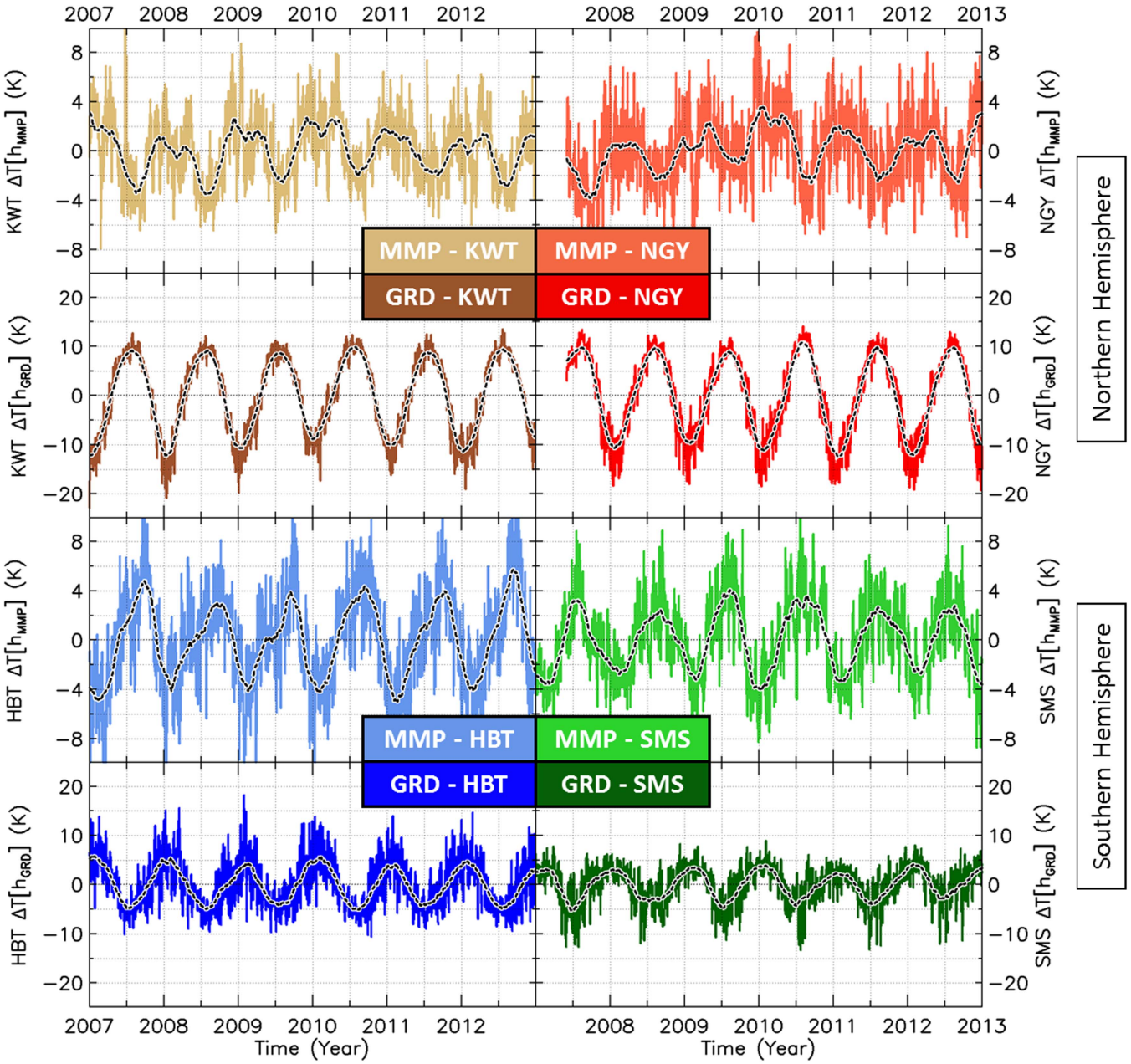


**Figure 3.** Temperature deviation from the mean value observed near the ground ($\Delta T\,[h_{\rm GRD}]$) and close to maximum muon production altitude ($\Delta T\,[h_{\rm MMP}]$) in the region of each detector. On the left side, the first two boxes from top to bottom show $\Delta T\,[h_{\rm MMP}]$ (light brown curve) and $\Delta T\,[h_{\rm GRD}]$ (dark brown curve) observed above the KWT detector. The last two boxes show $\Delta T\,[h_{\rm MMP}]$ (light blue curve) and $\Delta T\,[h_{\rm GRD}]$ (dark blue curve) observed above the HBT detector. On the right side, the first two boxes from top to bottom show $\Delta T\,[h_{\rm MMP}]$ (light red curve) and $\Delta T\,[h_{\rm GRD}]$ (dark red curve) observed above the NGY detector. The last two boxes show $\Delta T\,[h_{\rm MMP}]$ (light green curve) and $\Delta T\,[h_{\rm GRD}]$ (dark green curve) observed above the SMS detector. The black dashed curves represent the 3 month running average of daily data (colored curves).

variation due to the temperature effect ($\Delta I_T$) as:

$$\Delta I_T = \alpha_{\rm ATE} * \Delta H\,[p],\ \ p = 100\ {\rm hPa} \qquad (2)$$

where $\alpha_{\rm ATE}$ is the atmospheric expansion temperature coefficient given in % km$^{-1}$, $\Delta H\,[p]$ is the altitude deviation in kilometers of an atmospheric layer with pressure equal to $p$. In this analysis, we consider the altitude changes of the 100 hPa isobar line, which is the level of MMP. The top panel of Figure 5 shows the altitude changes of this isobar on each detector location. In this figure, it is possible to see a seasonal variation of $H$ with maximum value during summer. In addition, we can see that the amplitude of this variation is not the same for all detectors. It is about 0.40, 0.30, 0.25 and 0.15 km for NGY, KWT, HBT, and SMS respectively.

In order to obtain $\alpha_{\rm ATE}$, we consider that the short-term variation of the muon intensity corrected by pressure ($\Delta I_{\rm PC}^{\rm SRT}$, which is shown in Figure 1) is mainly affected by atmospheric temperature changes rather than solar or interplanetary phenomena in the period of analysis. Thus, we calculated $\alpha_{\rm ATE}$ by a linear regression between daily values of $\Delta H$ of 100 hPa isobar and $\Delta I_{\rm PC}^{\rm SRT}$ observed between 2007 January and 2012 December. We can see the anticorrelation between both,

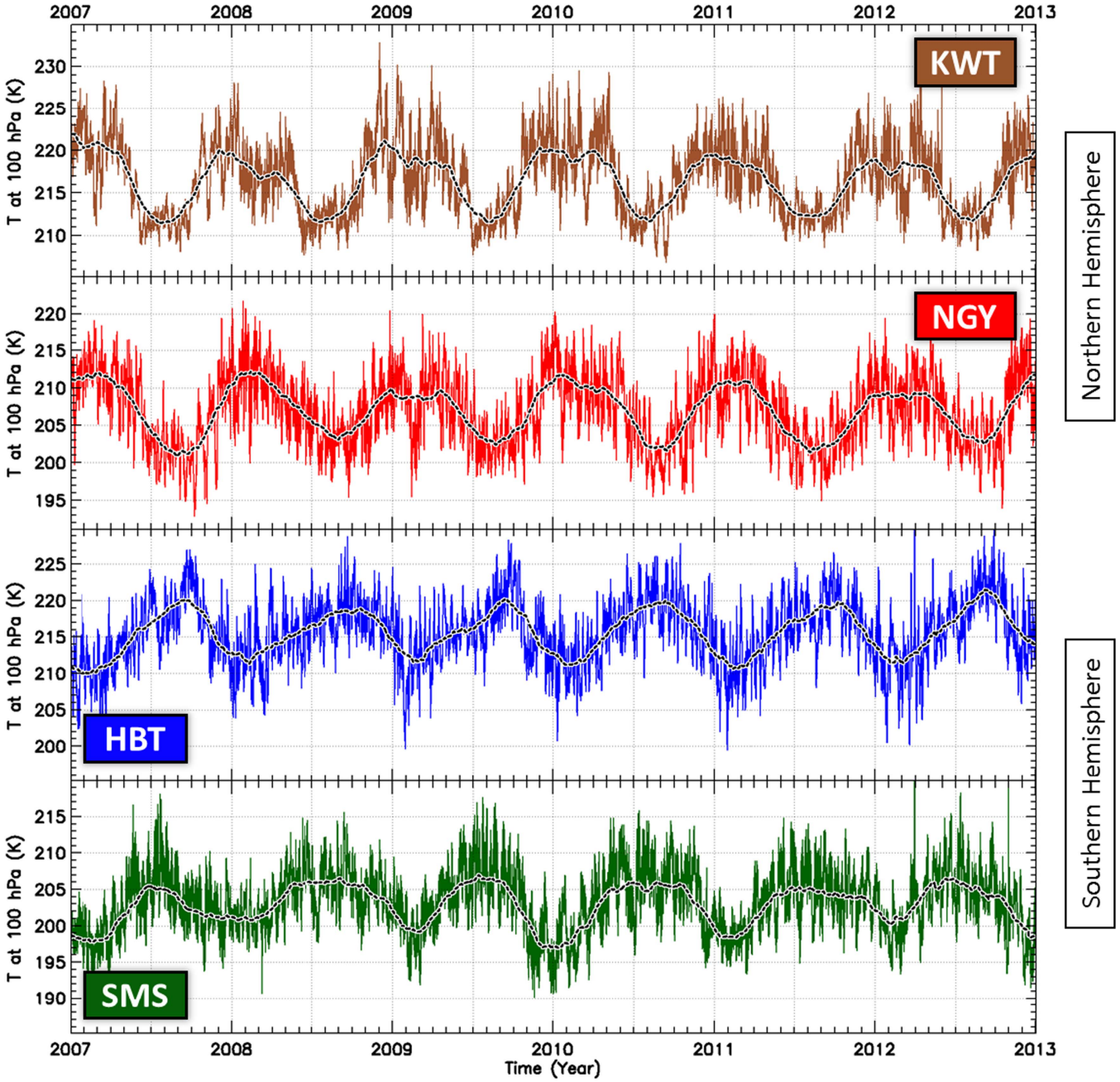


**Figure 4.** Temperature observed at 100 hPa isobar line on the KWT, NGY, HBT, and SMS detector locations from 2007 January until 2012 December. The colored curves show hourly data, while black dashed curves show the 3 month running average.

as well as the obtained values of $\alpha_{\rm ATE}$ and the linear Pearson correlation coefficient ($R$) in the bottom panel of Figure 5. All northern and southern hemisphere detectors present a good anticorrelation between $\Delta I_{\rm PC}^{\rm SRT}$ and $\Delta H$, but $R$ tends to be higher in the northern hemisphere detectors. Furthermore, the atmospheric expansion tends to produce a small muon intensity variation at ground detectors located in the southern hemisphere. While $\alpha_{\rm ATE}$ is of the order of $-6\%$ km$^{-1}$ in the northern hemisphere, it is about $-5\%$ km$^{-1}$ in the southern hemisphere.

### 4.2. The Ground (GRD) Method

This empirical method can be used as a simplified way to describe the temperature effect related to the atmospheric expansion phenomenon. As shown in Equation (3), it characterizes the muon intensity variation expected due to the temperature effect ($\Delta I_T$) as a linear function of temperature deviation close to the ground ($\Delta T\,[h_{\rm GRD}]$):

$$\Delta I_T = \alpha_{\rm GRD} * \Delta T\,[h_{\rm GRD}] \quad (3)$$

where $\alpha_{\rm GRD}$ is the ground temperature coefficient given in % K$^{-1}$. In our case, $h_{\rm GRD}$ is equal to 0.5 km of altitude. In Figure 3, we can see $\Delta T\,[h_{\rm GRD}]$ observed from 2007 January up to 2012 December for each GMDN detector location.

Similarly to what was done in the ATE method, we calculated $\alpha_{\rm GRD}$ through a linear regression between the short-term of the pressure corrected muon intensity variation ($\Delta I_{\rm PC}^{\rm SRT}$) and $\Delta T\,[h_{\rm GRD}]$ observed between 2007 January and

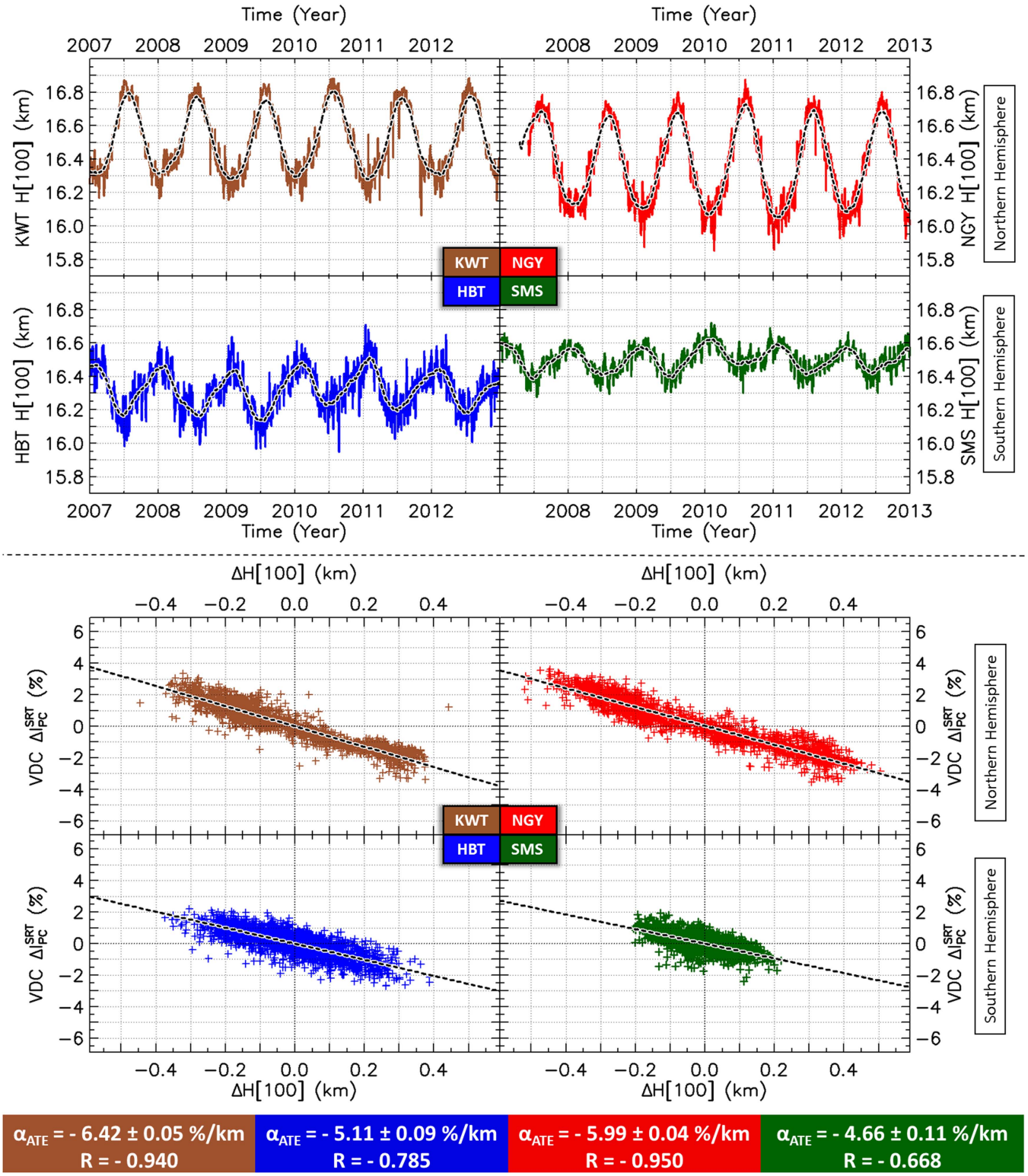


**Figure 5.** Top panel: altitude of 100 hPa isobar ($H$ [100]) observed from 2007 January until 2012 December above KWT, NGY, HBT, and SMS detectors. The black dashed curves show the 3 month running average of daily data (colored curves). On the bottom panel: linear correlation between daily data of the altitude deviation at 100 hPa ($\Delta H$ [100]) and the short-term pressure corrected muon intensity ($\Delta I_{PC}^{SRT}$) observed by VDCs of each detector. The atmospheric expansion temperature coefficient ($\alpha_{ATE}$) and linear Pearson correlation coefficients ($R$) obtained for each case are shown below the graphics.

2012 December. The linear regression and the values of ground temperature coefficients obtained for each detector are shown in Figure 6. In this figure, we can notice a significant difference between $\alpha_{GRD}$ of the NGY and SMS detectors. The ground temperature coefficient obtained for NGY is about twice as large as that obtained for SMS. We can also see that the Pearson product-moment correlation coefficient ($R$) is very close to 1.0 on the northern hemisphere detectors (KWT and

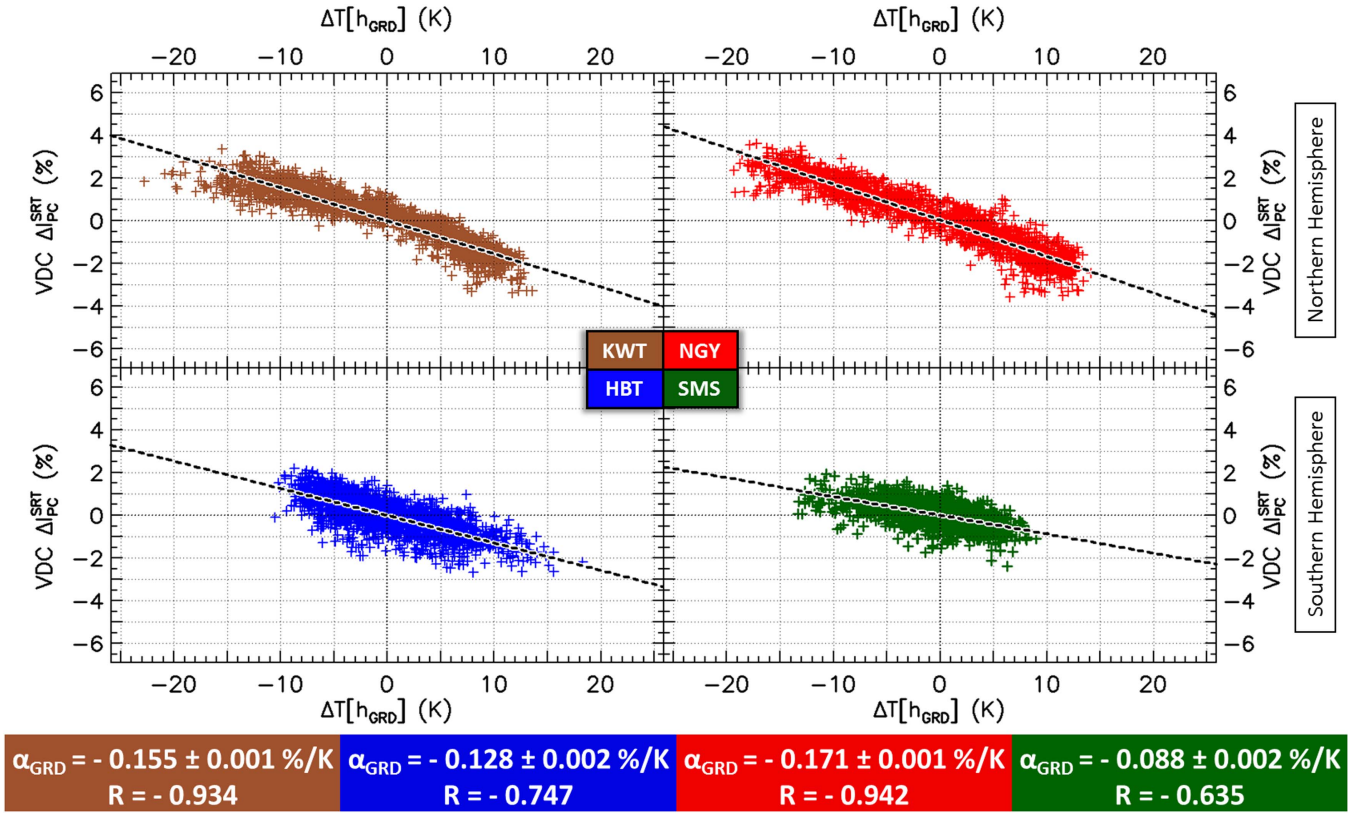


**Figure 6.** Linear correlation between the close to the ground temperature deviation ($\Delta T\,[h_{\rm GRD}]$) and the short-term pressure corrected muon intensity variation ($\Delta I_{\rm PC}^{\rm SRT}$) observed by the VDC of the KWT, NGY, HBT, and SMS detectors. The ground temperature coefficient ($\alpha_{\rm GRD}$) and the Pearson product-moment correlation coefficient ($R$) found for each detector are shown in the lower boxes.

NGY), while it is not too high ($R < 0.8$) on the southern hemisphere detectors (HBT and SMS).

### 4.3. The MMP Method

This empirical method describes the muon intensity variation expected due to the temperature effect ($\Delta I_T$) as a linear function of the temperature deviation observed near the altitude of MMP by pion decay ($\Delta T\,[h_{\rm MMP}]$):

$$\Delta I_T = \alpha_{\rm MMP} * \Delta T\,[h_{\rm MMP}] \quad (4)$$

where $\alpha_{\rm MMP}$ is the MMP temperature coefficient given in % $K^{-1}$ and $\Delta T\,[h_{\rm MMP}]$ is the temperature deviation at $h_{\rm MMP}$, which is the altitude of MMP on the cosmic ray shower. We assume $h_{\rm MMP}$ is equal to 16.5 km.

Similarly to what was done above, we calculated $\alpha_{\rm MMP}$ by a linear regression between the short-term muon intensity variation corrected by pressure ($\Delta I_{\rm PC}^{\rm SRT}$) and $\Delta T\,[h_{\rm MMP}]$. We can see the behavior of these two variables in Figures 1 and 3 respectively. In Figure 7 we show the correlation between them, as well as the obtained values of $\alpha_{\rm MMP}$ and the Pearson correlation coefficient ($R$). As can be seen in this figure, we found a positive correlation between $\Delta I_{\rm PC}^{\rm SRT}$ and $\Delta T\,[h_{\rm MMP}]$ for all detectors with $R$ around 0.7 and 0.5 for northern and southern hemisphere detectors, respectively. While $\alpha_{\rm MMP}$ on the southern hemisphere detectors has values of the order of 0.1% $K^{-1}$, it is of the order of 0.3% $K^{-1}$ on the northern detectors. Positive values of MMP temperature coefficients are also found in Duperier (1949), Trefall (1955a) and French & Chasson (1959), where cosmic ray intensity observed at sea level by ionization chambers and by gas scintillator cosmic ray detectors was compared to the temperature variation observed at isobar levels around 100 mb.

### 4.4. The GRD, ATE and MMP Method Combinations (GRD +MMP and ATE+MMP)

While the GRD and ATE methods are associated with the negative temperature effect, the MMP method is associated with the positive temperature effect. Therefore, we consider only part of the temperature effect when using one of these methods alone. In order to study both effects together, we analyzed combinations of these methods.

We analyzed the combination of the ATE and MMP methods, which is generally referred to as the Effective Level of Generation Method according to Berkova et al. (2011). In this paper, for simplicity, we use the term ATE+MMP. As we can see in Equation (5), this method describes the muon intensity variation expected due to the temperature effect ($\Delta I_T$) by the sum of Equations (2) and (4):

$$\Delta I_T = \sigma_{\rm ATE} * \Delta H\,[p] + \sigma_{\rm MMP} * \Delta T\,[h_{\rm MMP}] \quad (5)$$

where $\sigma_{\rm ATE}$ is the atmospheric expansion temperature coefficient given in % $km^{-1}$, $\Delta H\,[p]$ is the altitude deviation in kilometers of an atmospheric layer with pressure equal to $p$ (in our case 100 hPa), $\alpha_{\rm MMP}$ is the MMP temperature coefficient given in % $K^{-1}$ and $\Delta T\,[h_{\rm MMP}]$ is the temperature deviation at $h_{\rm MMP}$ (16.5 km). We also analyzed the combination of the

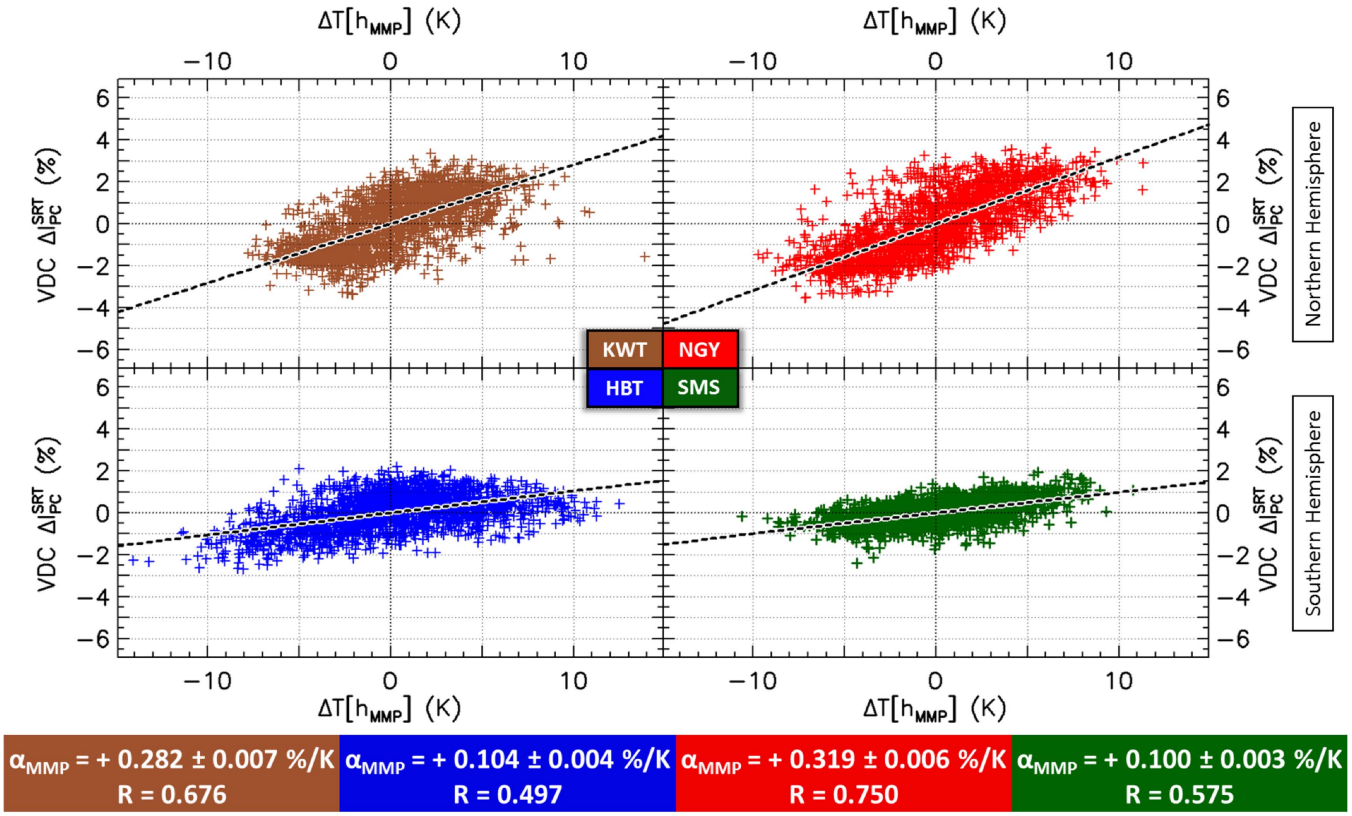


**Figure 7.** Linear correlation between the temperature deviation at the altitude of maximum muon production by pion decay ($\Delta T\,[h_{\rm MMP}]$) and the short-term pressure corrected muon intensity ($\Delta I_{\rm PC}^{\rm SRT}$) observed by the VDC of the KWT, NGY, HBT, and SMS detectors. The maximum muon production temperature coefficient ($\alpha_{\rm MMP}$) and the Pearson product-moment correlation coefficient ($R$) found for each detector are shown in the lower boxes.

**Table 1**
Values of ATE ($\sigma_{\rm ATE}$), MMP ($\sigma_{\rm MMP}$) and GRD ($\sigma_{\rm GRD}$) Temperature Coefficients Found for ATE+MMP and GRD+MMP Methods

| Detector | $\sigma_{\rm ATE}$ (%/km) | $\sigma_{\rm MMP}$ (%/K) | $\frac{\sigma_{\rm ATE}-\alpha_{\rm ATE}}{\alpha_{\rm ATE}} * 100$ (%) | $\frac{\sigma_{\rm MMP}-\alpha_{\rm MMP}}{\alpha_{\rm MMP}} * 100$ (%) |
|---|---|---|---|---|
| ATE+MMP Method | | | | |
| KWT | −6.17 ± 0.07 | +0.022 ± 0.004 | −03.9 | −92.2 |
| NGY | −5.51 ± 0.06 | +0.043 ± 0.004 | −08.0 | −86.5 |
| HBT | −4.67 ± 0.10 | +0.027 ± 0.003 | −08.6 | −74.0 |
| SMS | −3.50 ± 0.14 | +0.044 ± 0.002 | −24.9 | −56.0 |
| GRD+MMP Method | | | | |
| KWT | −0.140 ± 0.002 | +0.060 ± 0.004 | −09.7 | −78.7 |
| NGY | −0.150 ± 0.002 | +0.070 ± 0.004 | −12.3 | −78.1 |
| HBT | −0.122 ± 0.003 | +0.012 ± 0.004 | −04.7 | −88.7 |
| SMS | −0.062 ± 0.003 | +0.053 ± 0.004 | −29.5 | −47.0 |

GRD and MMP methods. In this case, $\Delta I_T$ is described as:

$$\Delta I_T = \sigma_{\rm GRD} * \Delta T\,[h_{\rm GRD}] + \sigma_{\rm MMP} * \Delta T\,[h_{\rm MMP}] \qquad (6)$$

where $\sigma_{\rm GRD}$ is the ground temperature coefficient given in % $K^{-1}$ and $\Delta T\,[h_{\rm GRD}]$ is the deviation of the temperature measured close to the ground ($h_{\rm GRD} = 0.5$ km).

The values obtained for each case through a multiple linear regression between muon and atmospheric data are shown in Table 1. As we can see in the last two columns on the right, the temperature coefficients obtained considering the positive and negative effects together ($\sigma$) are lower than that obtained when we consider only one effect alone ($\alpha$). For the KWT, NGY and HBT detectors, the decrease of the MMP coefficients (positive effect) is much more expressive than that observed in the coefficients related to the negative effect (ATE and GRD coefficients). For the SMS detector, the decrease of $\sigma_{\rm MMP}$ in comparison with $\alpha_{\rm MMP}$ is also higher than the decrease shown by the GRD and ATE coefficients. However, this difference is not as significant as it is in the other detectors. This situation can be clearly seen by looking at the obtained values of $\sigma_{\rm GRD}$ and $\sigma_{\rm MMP}$ coefficients. While the first one is at least twice as high as the second for KWT, NGY and HBT, they practically have the same value for SMS.

### *4.5. The Theoretical (THR) Method and its Variation (THR-L)*

The theoretical method, which is also called the integral method, considers the theory of the temperature effect, as was shown by Sagisaka (1986). In this method, we can write the

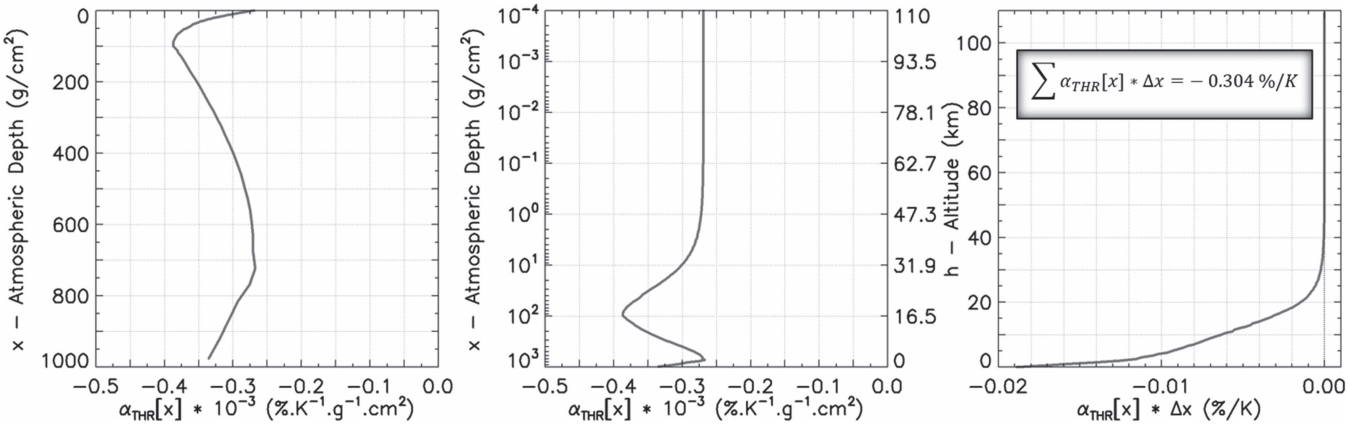


**Figure 8.** Left panel, the theoretical partial temperature coefficient ($\alpha_{\rm THR}[x]$) for 0° zenith angle and 0.32 GeV muon threshold energy calculated by Sagisaka (1986) along a linear atmospheric depth axis. Middle panel, $\alpha_{\rm THR}[x]$ for same zenith angle and muon threshold energy along a linear altitude (logarithmic atmospheric depth) axis. Right panel, the product between $\alpha_{\rm THR}[x]$ and the atmospheric depth variation ($\Delta x$) observed in each atmospheric layer with 0.5 km of altitude range.

muon intensity variation due to the temperature effect ($\Delta I_T$) as:

$$\Delta I_T = \int_0^{x_{\rm GRD}} \alpha_{\rm THR}[x] * \Delta T[x] * dx \qquad (7)$$

where $\Delta T[x]$ is the temperature deviation; $dx$ is the differential atmospheric depth given in g cm$^{-2}$; and $\alpha_{\rm THR}[x]$, given in % K$^{-1}$ g$^{-1}$ cm$^2$, is the theoretical partial temperature coefficient, which was calculated using a muon generation and decay theory and depends on the energy threshold and the zenith angle of muons arriving at a given detector. The integration was done from the top of the atmosphere ($x = 0$) to the ground ($x_{\rm GRD}$). In this work, we used the Boole's rule method for calculating the integrals.

We obtained the atmospheric depth profile ($x[h]$) using Equation (8). We calculated an average atmospheric depth profile using daily atmospheric temperature and pressure data observed between 0.5 and 110 km of altitude in atmospheric layers with 0.5 km of thickness. As expected, we found a negative exponential function behavior of $x[h]$ with altitude:

$$x[h] = \int_h^{\infty} \rho[h]dh, \quad \rho[h] = \frac{P[h]}{T[h]} * \frac{M_{\rm Mol}}{R} \qquad (8)$$

where $P[h]$, $T[h]$ and $\rho[h]$ are respectively the atmospheric pressure, the atmospheric temperature and the air density at a given altitude $h$; $M_{\rm Mol}$ is the molar mass of air and $R$ is the universal gas constant.

Unlike the other methods analyzed in this work, whose energy and zenith angle dependence of the temperature coefficients are given empirically, in the theoretical method we need to choose the adequate coefficient according to the muon detector characteristics. Considering the aspects of the VDC of the HBT, KWT, NGY and SMS detectors, we chose $\alpha_{\rm THR}[x]$ calculated by Sagisaka (1986) considering a 0° zenith angle and muon threshold energy equal to 0.32 GeV. We can see how this coefficient varies with the atmospheric depth in the left plot of Figure 8. We can also see $\alpha_{\rm THR}[x]$ for this zenith angle and muon threshold energy, as well as for other angles and energy thresholds in Figure 3 of Sagisaka (1986). The middle plot of Figure 8 shows how the theoretical partial temperature coefficient varies with the altitude. The right plot shows the behavior of the product between $\alpha_{\rm THR}[x]$ and $\Delta x$, which is the difference between the atmospheric depth obtained in an atmospheric layer at a given altitude ($x[h_i]$) and the one obtained in the next layer above it ($x[h_{i+1}]$). The sum of this product for all layers gives the theoretical total temperature coefficient, which in our case is $-0.304\%$ K$^{-1}$.

Once $\alpha_{\rm THR}[x]$ calculated by Sagisaka (1986) does not present explicitly local dependences, we consider the same values of partial temperature coefficients for all detectors in the THR method. In order to check local influences, we created the THR-L method, which considers the muon intensity variation associated with the temperature effect ($\Delta I_T$) equal to:

$$\Delta I_T = L * \Delta I_T^{\rm THR} \qquad (9)$$

where $\Delta I_T^{\rm THR}$ is the muon intensity variation expected in a detector due to the temperature effect calculated using the THR method ($\Delta I_T$ on Equation (7)) and $L$ is the local coefficient of this detector. We calculated $L$ by a linear regression between the short-term muon intensity variation corrected by pressure ($\Delta I_{\rm PC}^{\rm SRT}$) and $\Delta I_T^{\rm THR}$. We found $L$ equal to 0.940 for KWT, 0.904 for NGY, 0.712 for HBT and 0.673 for SMS. An $L$ value close to 1.0 means a good agreement between the observed muon intensity and the one calculated by the THR method. In this way, $L \cong 1$ for the northern hemisphere detectors indicates a good reproduction of the temperature effect in these detectors by THR method. However, $L \leqslant 0.7$ values on the HBT and SMS detectors may indicate an insufficient reproduction of the temperature effect by the THR method on the southern hemisphere detectors. It can also indicate the existence of a local phenomenon not related to the temperature or the pressure effects, which is more prominent in the south than in the north hemisphere.

### 4.6. The Mass Weighted (MSS) Method

This method was developed by an approximation of the THR method and it has been used in some studies (Yanchukovsky et al. 2007; Berkova et al. 2011). In the MSS method, we can write the muon intensity variation due to the temperature effect ($\Delta I_T$) as:

$$\Delta I_T = \alpha_{\rm MSS} * \Delta T_{\rm MSS} \qquad (10)$$

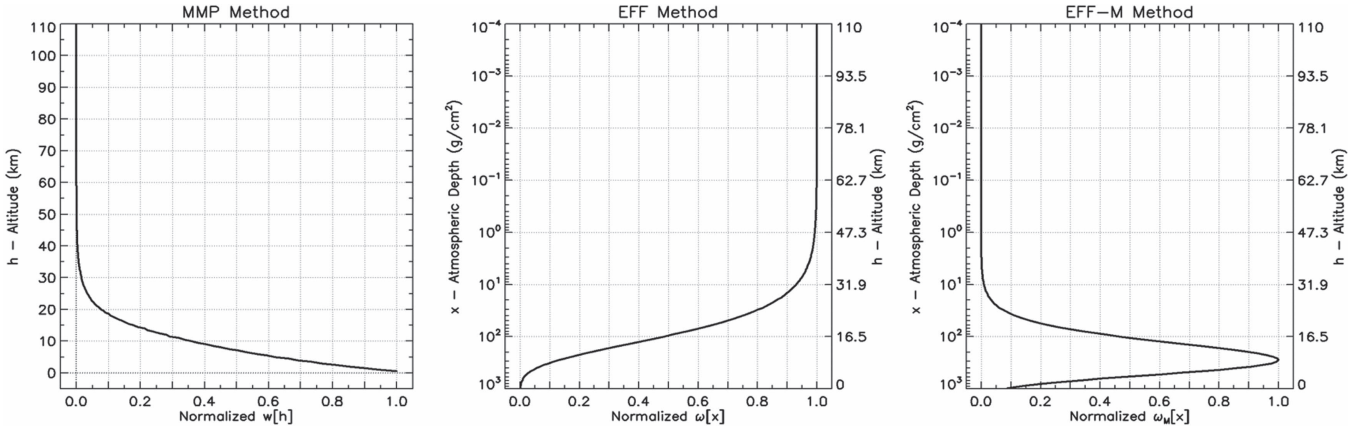


**Figure 9.** Left graphic: mass weighted function ($w[h]$) normalized by its maximum value. Middle graphic: weight function of the effective temperature method ($\omega[x]$) normalized by its maximum value. Right graphic: weight function of the modified effective temperature method ($\omega_M[x]$) normalized by its maximum values. The behavior of all curves is shown along a logarithmic atmospheric depth (linear altitude) axis.

$$T_{\rm MSS} = \sum_{i=0}^{n} w[h_i] * T[h_i], \quad w[h_i] = \frac{x[h_i] - x[h_{i+1}]}{x[h_0]} \tag{11}$$

where $\alpha_{\rm MSS}$ is the mass weighted temperature coefficient given in % $K^{-1}$; $\Delta T_{\rm MSS}$ is the deviation of the mass weighted temperature; $w[h]$ is the air mass weighted function; $T[h_i]$ is the temperature in kelvin observed at the altitude $h_i$; $x[h_i]$ is the atmospheric depth at the same altitude; $h_0$ is the closest to ground altitude (in this work, 0.5 km); $h_n$ is the altitude closest to the top of the atmosphere (in this work, 110 km). We considered that $x[h_{n+1}]$ is equal to zero. As can be seen in the left graphic of Figure 9, $w[h]$ has the same behavior as the atmospheric depth, i.e., it has a maximum value near the ground and exponentially decreases with altitude. The top panel of Figure 10 shows $T_{\rm MSS}$ obtained for each GMDN detector location using Equation (11). In this figure, we can see a seasonal variation on $T_{\rm MSS}$, which presents maximum amplitude during summertime for all detectors.

The MSS method has a unique temperature coefficient that takes into account the temperature effect in the entire atmosphere. However, differently from the THR method, its temperature coefficient ($\alpha_{\rm MSS}$) is different for each detector. This coefficient was calculated using a linear regression between the short-term muon intensity variation corrected by pressure ($\Delta I_{\rm PC}^{\rm SRT}$) and $\Delta T_{\rm MSS}$. The bottom panel of Figure 10 shows the obtained linear regressions between both, as well as the values of $\alpha_{\rm MSS}$ and the linear Pearson correlation coefficient ($R$) found for each detector. We can see in this figure that both northern and southern hemisphere detectors present a good correlation coefficient. In a first-order approximation, the northern detectors show $\alpha_{\rm MSS}$ equal to 0.3% $K^{-1}$, while the southern hemisphere detectors show $\alpha_{\rm MSS}$ equal to 0.2% $K^{-1}$.

We observed that the obtained values of $\alpha_{\rm MSS}$ are very similar to the product between the theoretical total temperature coefficient and the local effect coefficient ($L$) calculated for each detector in the THR and THR-L methods. In other words, looking at the MSS, THR and THR-L methods, we notice that:

$$\alpha_{\rm MSS} \cong L * \int_0^{x_{\rm GRD}} \alpha_{\rm THR}[x]dx \tag{12}$$

As already shown above, $L$ is equal to 0.940 for KWT, 0.904 for NGY, 0.712 for HBT and 0.673 for SMS, and the theoretical total temperature coefficient is equal to $-0.304\%$ $K^{-1}$. Thus, the product between both is $-0.285\%$ $K^{-1}$ for KWT, $-0.274\%$ $K^{-1}$ for NGY, $-0.216\%$ $K^{-1}$ for HBT and $-0.205\%$ $K^{-1}$ for SMS, which are similar to $\alpha_{\rm MSS}$ found for each detector. Based on these results, we can consider the MSS method to be practically equal to the THR-L method, i.e., we can consider the MSS method as an approximation of the THR method that takes into account local effects or differences in the atmosphere configuration from one place to another.

### 4.7. The Effective Temperature (EFF) Method and its Variation (EFF-M)

This method was shown by Barrett et al. (1952) and, in its upgraded form, by Ambrosio et al. (1997). It was developed taking into account the temperature effect on high-energy (underground) muon detectors. Just out of curiosity, we analyzed how this method works for ground muon detectors.

In a similar way that was done in the MSS method, the EFF method considers the entire atmospheric temperature profile using a unique parameter, called effective temperature ($T_{\rm EFF}$), which is calculated through a weight function. However, this weight function is related to pion and nucleon absorption in the atmosphere. As shown in Equation (13), the muon intensity variation due to the temperature effect ($\Delta I_T$) in this method is described as a linear function of $T_{\rm EFF}$, which is described by Equation (14) shown below and by Equation (5) of Ambrosio et al. (1997).

$$\Delta I_T = \alpha_{\rm EFF} * \Delta T_{\rm EFF} \tag{13}$$

$$T_{\rm EFF} = \frac{\int_0^{x_{\rm GRD}} \omega[x] * T[x]dx}{\int_0^{x_{\rm GRD}} \omega[x]\,dx}, \quad \omega[x] = \frac{1}{x} * (e^{-\frac{x}{\lambda_\pi}} - e^{-\frac{x}{\lambda_n}}) \tag{14}$$

where $\alpha_{\rm EFF}$ is the effective temperature coefficient given in % $K^{-1}$; $\Delta T_{\rm EFF}$ is the deviation from the effective temperature; $\omega[x]$ is the weight function; $T[x]$ is the temperature observed at an atmospheric depth $x$; $x_{\rm GRD}$ is the atmospheric depth at ground; $\lambda_\pi$ and $\lambda_n$ are respectively the atmospheric attenuation length for pions and for nucleons, which are equal to 160 and 120 g $cm^{-2}$. As we can see in the middle graphic of Figure 9, $\omega[x]$ gives more importance to temperatures observed above 30 km. The behavior of $T_{\rm EFF}$ calculated for

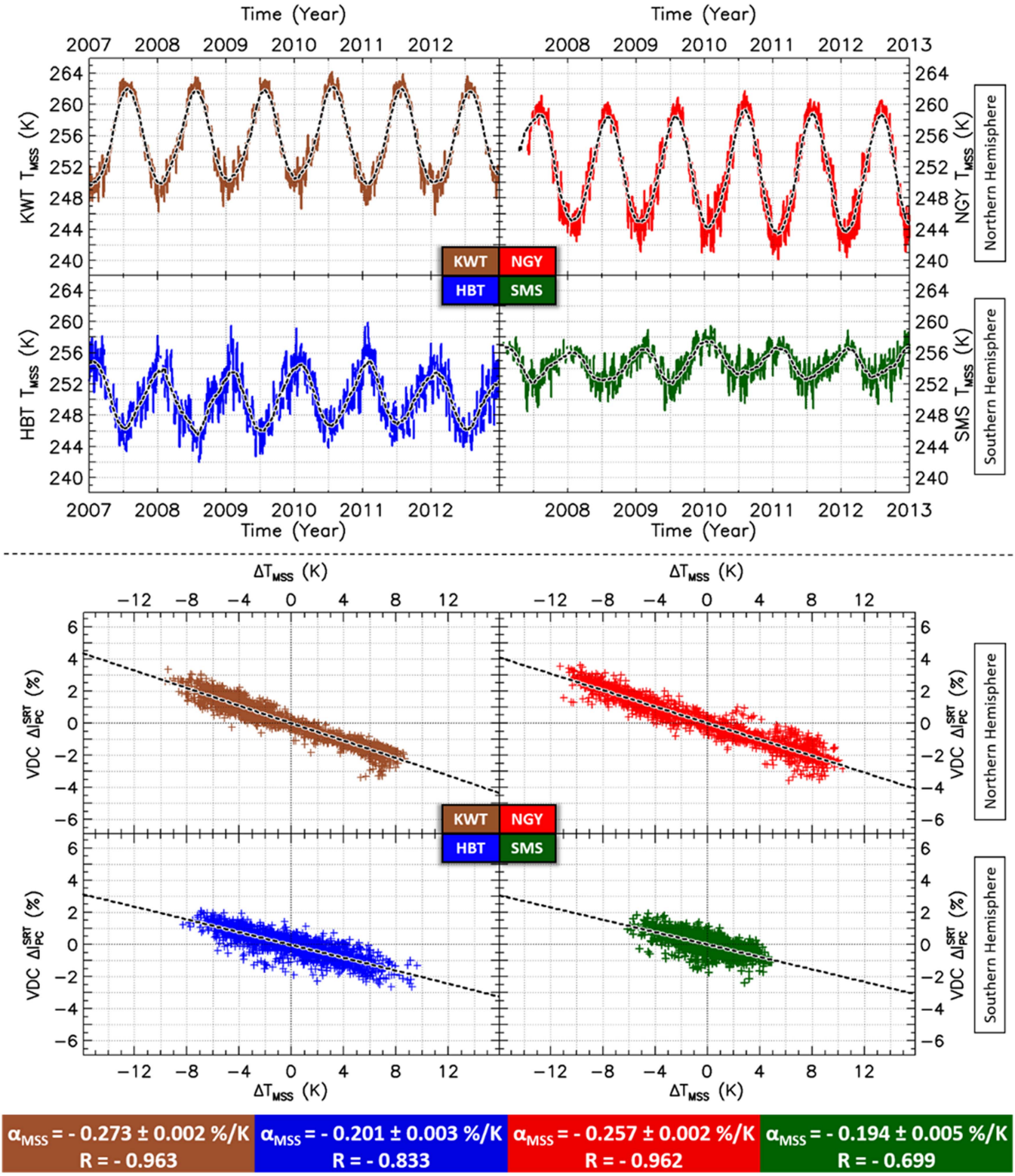


**Figure 10.** Top panel: mass weighted temperature ($T_{\rm MSS}$) obtained from 2007 January until 2012 December for the KWT, NGY, HBT, and SMS detectors. The colored curves show daily data and the black dashed curves show the 3 month running average of this data. Bottom panel: linear correlation between the deviation of mass weighted temperature ($\Delta T_{\rm MSS}$) and the short-term pressure corrected muon intensity ($\Delta I_{\rm PC}^{\rm SRT}$) observed by vertical directional channels (VDC) of each detector. The mass weighted temperature coefficients ($\alpha_{\rm MSS}$) and linear Pearson correlation coefficients ($R$) obtained in each case are shown below the graphics.

each detector location using data observed between 2007 January and 2012 December is shown in the top panel of Figure 11. In this figure, we cannot see a seasonal variation on $T_{\rm EFF}$ obtained for SMS, unlike what happens for the other detectors, where we can observe a seasonal variation with maximum during the summer.

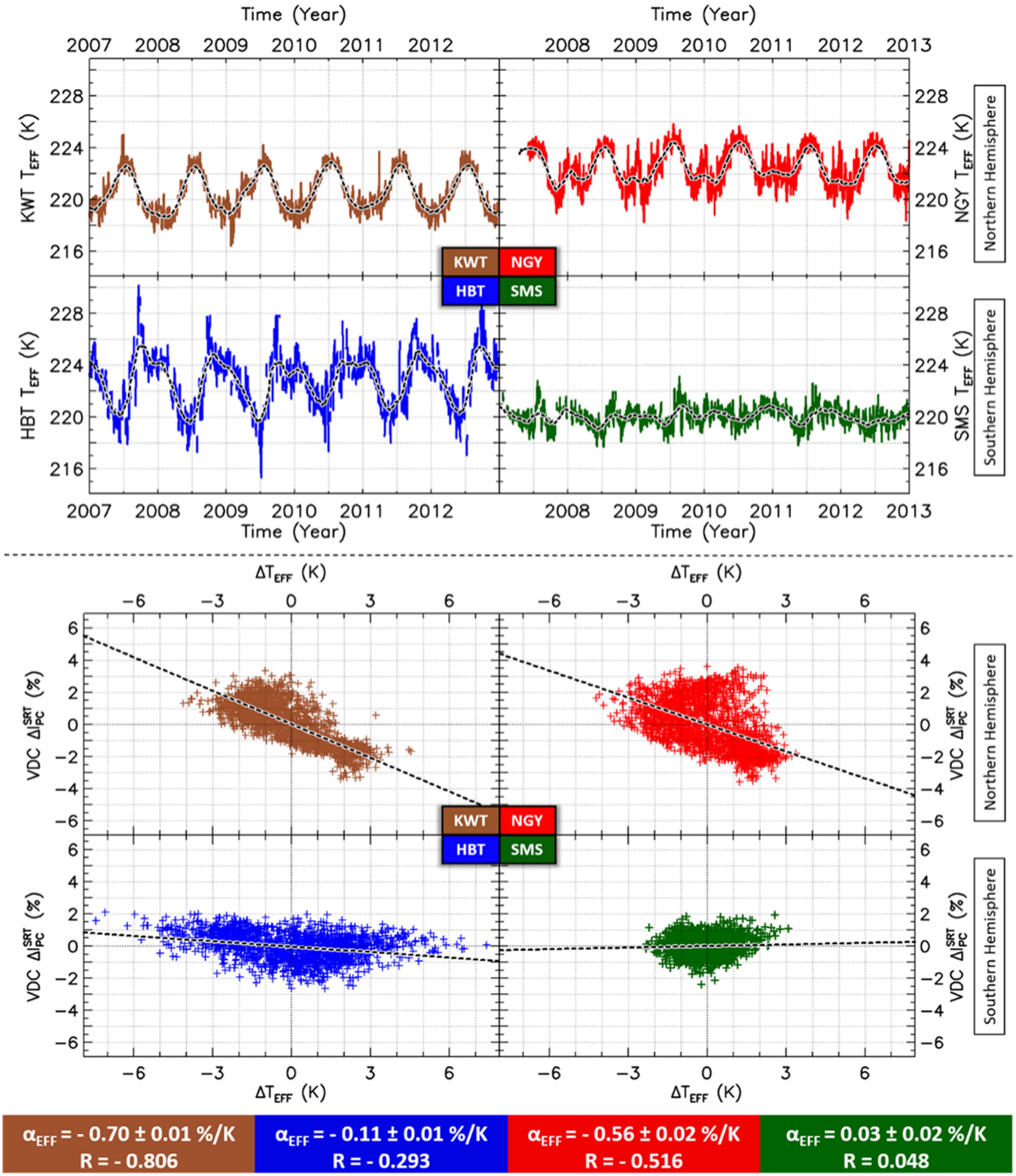


**Figure 11.** Top panel: effective temperature ($T_{EFF}$) obtained from 2007 January until 2012 December above the KWT, NGY, HBT, and SMS detectors. The black dashed curves show the 3 month running average of the daily data (colored curves). Bottom panel: correlation between the short-term pressure corrected muon intensity ($\Delta I_{PC}^{SRT}$) observed by the vertical directional channels (VDC) of each detector and the deviation of the effective temperature ($\Delta T_{EFF}$). Below the graphics, the effective temperature ($\alpha_{EFF}$) and linear Pearson correlation ($R$) coefficients obtained are shown for each case.

The bottom panel of Figure 11 shows the correlation between the short-term pressure corrected muon intensity variation ($\Delta I_{PC}^{SRT}$) and $T_{EFF}$ obtained for each detector, which is used to calculate the effective temperature coefficient ($\alpha_{EFF}$). As we can see in this figure, $\Delta I_{PC}^{SRT}$ and effective temperature data have an anticorrelation, at least reasonable, on the northern hemisphere detectors. We only found a good and clear anticorrelation, i.e., a linear Pearson correlation coefficient

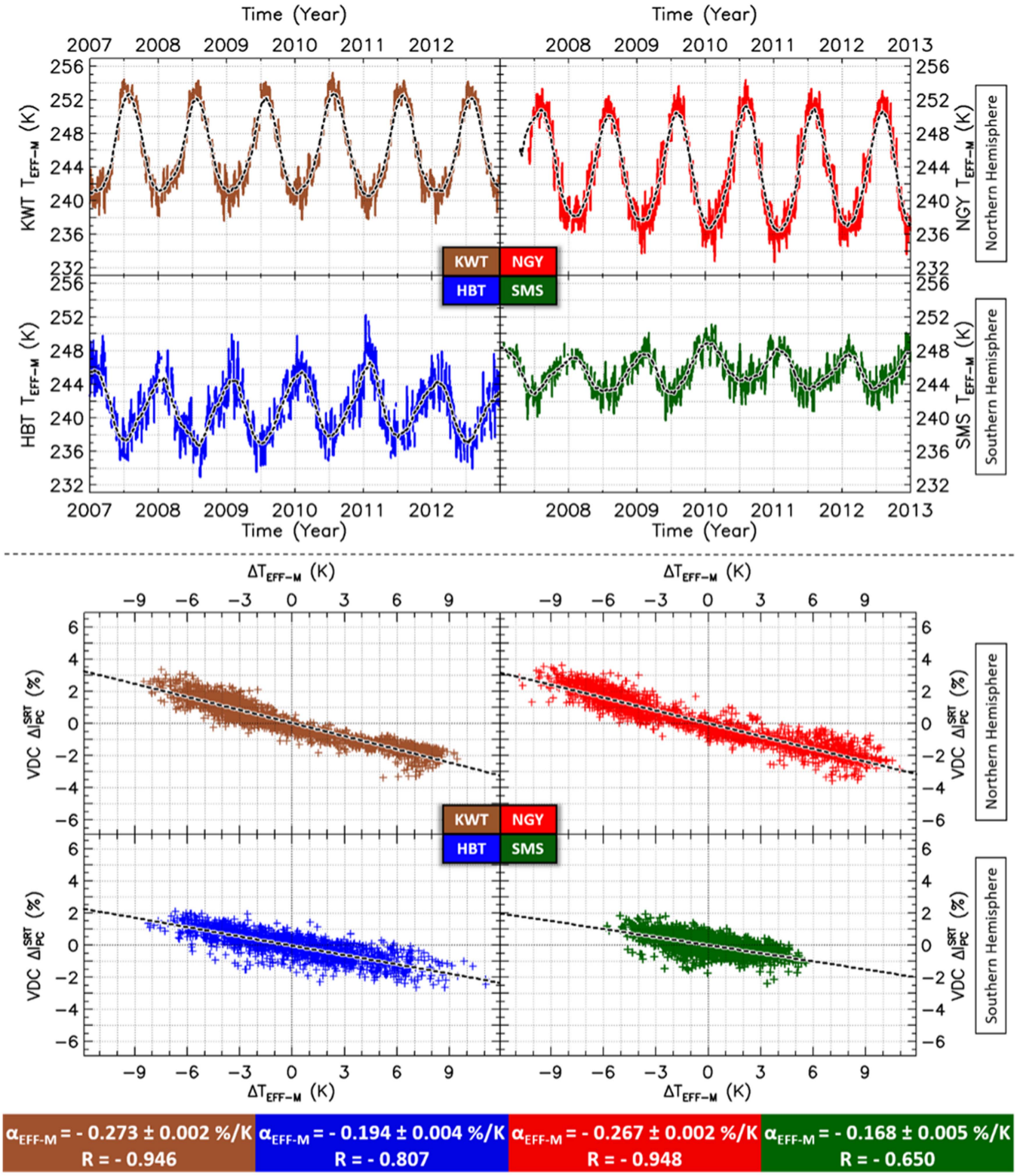


**Figure 12.** Top panel: modified effective temperature ($T_{\mathrm{EFF}-M}$) observed above each GMDN detector from 2007 January until 2012 December. Bottom panel: correlation between the short-term pressure corrected muon intensity variation ($\Delta I_{\mathrm{PC}}^{\mathrm{SRT}}$) observed by the VDCs of the KWT, NGY, HBT and SMS detectors and the deviation of modified effective temperature ($\Delta T_{\mathrm{EFF}-M}$). The modified effective temperature coefficient ($\alpha_{\mathrm{EFF}-M}$) and linear Pearson correlation coefficient ($R$) obtained using each detector data are shown below the graphics.

($R$) lower than −0.8, for KWT. We found $R$ equal to −0.516 on NGY, which like KWT is located in the northern hemisphere. On detectors located on the southern hemisphere (HBT and SMS) we found a weak correlation ($|R| < 0.3$).

It was found that better results would arise if we modified the weight function as shown in Equation (15). In this way, we created the modified temperature effective (EFF-M) method. As we can see in the right graphic of Figure 9, the modified

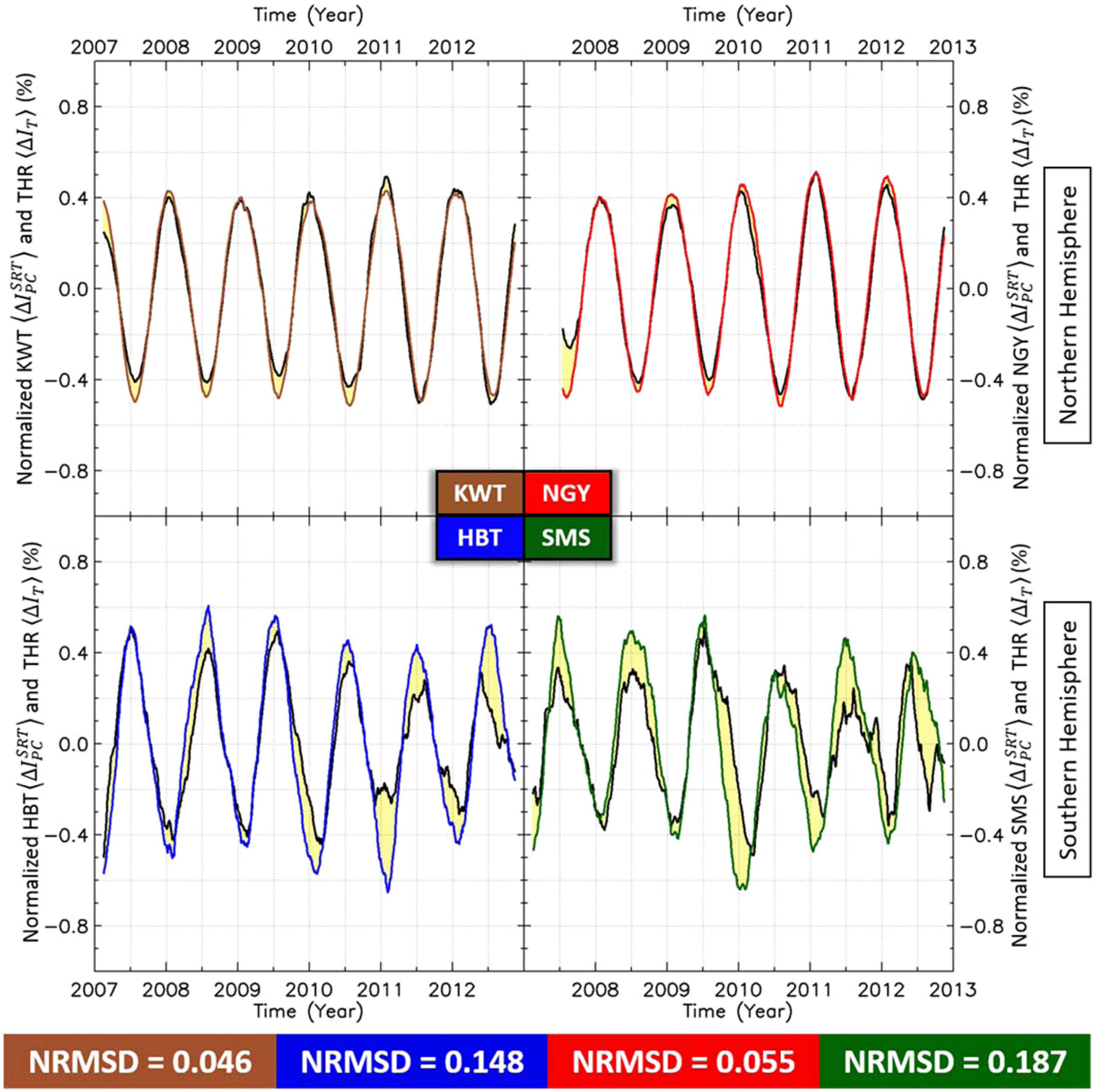


**Figure 13.** Comparison between the 3 month running average of the short-term measured muon intensity variation corrected by pressure ($\langle \Delta I_{\rm PC}^{\rm SRT} \rangle$) and the 3 month running average of expected muon intensity variation due the temperature effect calculated by the theoretical method (THR $\langle \Delta I_T \rangle$). The black curves represent the observed data, while the colored curves represents the expected data. The yellow areas highlight the difference between observed and the expected muon intensity seasonal variation. The normalized root-mean-square deviations (NRMSDs) found for each detector are shown in the bottom. All plotted data are normalized by their maximum value, in order to obtain a similar seasonal variation amplitude for all detectors.

weight function ($\omega_M[x]$) takes into account (i.e., is higher than 0.5 for) temperatures measured between 5 and 16.5 km.

$$T_{\rm EFF-M} = \frac{\int_0^{x_{\rm GRD}} \omega_M[x] * T[x] dx}{\int_0^{x_{\rm GRD}} \omega_M[x]\, dx}, \quad \omega_M[x] = x * (e^{-\frac{x}{\lambda_\pi}} - e^{-\frac{x}{\lambda_n}}) \quad (15)$$

where $T_{\rm EFF-M}$ is the modified effective temperature, $T[x]$ is the temperature observed at an atmospheric depth $x$; $x_{\rm GRD}$ is the atmospheric depth at ground; $\omega_M[x]$ is the modified weight function; $\lambda_\pi = 160\ {\rm g\ cm^{-2}}$ and $\lambda_n = 120\ {\rm g\ cm^{-2}}$ are respectively the atmospheric attenuation lengths for pions and nucleons. As we can see in the Figure 12, differently from the original effective temperature, $T_{\rm EFF-M}$ presents a clear seasonal variation with maximum amplitude during summertime on all detector locations. As we can also see in this figure, the absolute values of linear Pearson correlation coefficients ($R$) obtained through correlation between the $\Delta I_{\rm PC}^{\rm SRT}$ and $T_{\rm EFF-M}$ are higher than 0.6 for all detectors. In other words, we found a better correlation between muon intensity and atmospheric temperature data using $\omega_M[x]$

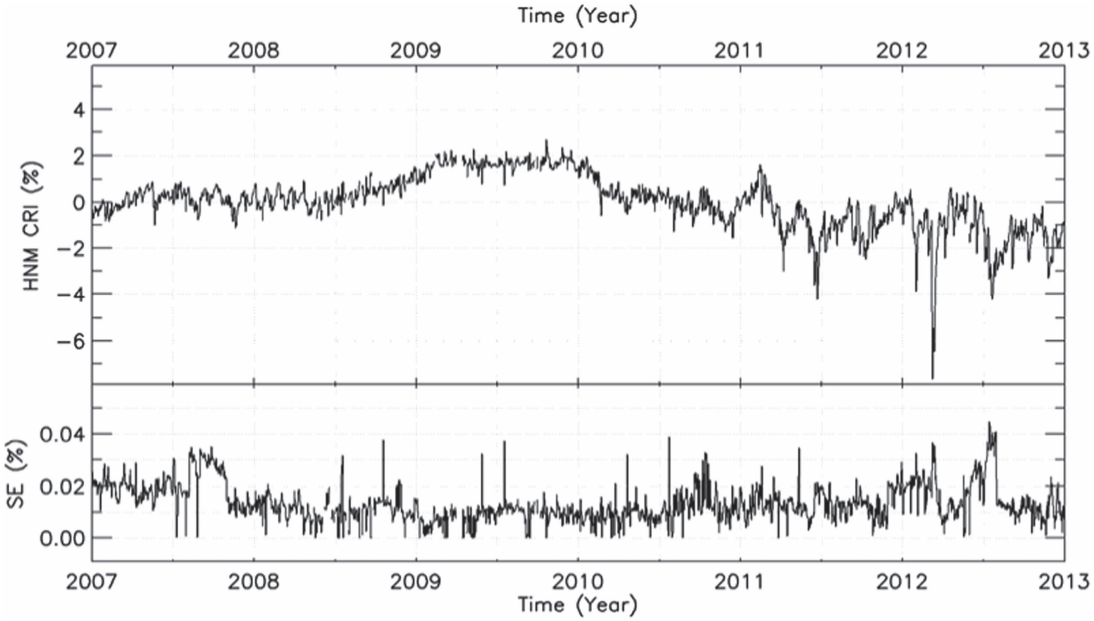


**Figure 14.** Daily mean high-energy neutron monitors ($R_c > 6\ GV$) cosmic ray intensity variation (HNM CRI) observed from 2007 January up to 2012 December. The bottom graphic shows the standard error (SE) deduce from hourly data for each value shown in the top graphic.

instead $\omega[x]$. We can also see in this figure that the obtained values of effective temperature coefficients ($\alpha_{\mathrm{EFF}-M}$) are very similar to the obtained by the MSS method ($\alpha_{\mathrm{MSS}}$).

## 5. COMPARISON BETWEEN RESULTS OBTAINED FROM EACH METHOD

In order to compare the methods analyzed in this work, we looked at how the variation of muon intensity variation expected due to the temperature effect ($\Delta I_T$) obtained by each method is similar to the seasonal variation observed on the measured data. We calculated, for each method, the normalized root-mean-squared deviation (NRMSD) between the three-month moving average of the short-term muon intensity corrected by pressure ($\langle \Delta I_{\mathrm{PC}}^{\mathrm{SRT}} \rangle$) and the three-month moving average of the muon intensity variation expected due to the temperature effect ($\langle \Delta I_T \rangle$) using Equation (16). The lower the value of NRMSD, the higher the similarity between observed and calculated data. For example, as we can see in Figure 13, the NRMSD of the THR method obtained for NGY and KWT is lower than that found for HBT and SMS, since THR $\langle \Delta I_T \rangle$ is more similar to $\langle \Delta I_{\mathrm{PC}}^{\mathrm{SRT}} \rangle$ on the northern than on the southern detectors. Although there is a high similarity between the expected and observed NGY data most of the time, the NRMSD for this detector is bigger than that found for KWT. This is due to the high discrepancy between THR $\langle \Delta I_T \rangle$ and $\langle \Delta I_{\mathrm{PC}}^{\mathrm{SRT}} \rangle$ observed above NGY in mid-2007. We confirmed that this significant discrepancy is not related to the data gap existing between 2007 January and May. It is probably due to a failure of the theoretical method in reproducing the muon intensity variation based in the behavior of the atmospheric temperature profile observed in this period weighted along the altitude by the theoretical temperature coefficient. When we changed this weighting through other methods, this discrepancy increased or decreased depending on the method. The same occurs for the large discrepancy that can be observed at the beginning of 2011 in the HBT graphic and for those present in the SMS data. Moreover, for some methods, new significant discrepancies appear on different periods. Furthermore, a small part of the discrepancy between observed and calculated data can be related to a non-complete removal of extraterrestrial effects on the measured muon data:

$$\mathrm{NRMSD} = \frac{\sqrt{\frac{1}{n}\sum_{i=0}^{n}(\langle \Delta I_{\mathrm{PC}}^{\mathrm{SRT}} \rangle - \langle \Delta I_T \rangle)^2}}{\max[\langle \Delta I_{\mathrm{PC}}^{\mathrm{SRT}} \rangle] - \min[\langle \Delta I_{\mathrm{PC}}^{\mathrm{SRT}} \rangle]}. \quad (16)$$

Retaining the purpose of comparing the different methods for describing the temperature effect studied in this work, we analyzed the correlation between the pressure corrected neutron monitor data and the muon intensity corrected by temperature and pressure effects ($\Delta I_{\mathrm{TPC}}$). We expect that the variation of $\Delta I_{\mathrm{TPC}}$ relating to solar cycle is similar to the behavior of cosmic ray data recorded by the neutron monitors, which practically are not affected by temperature effects. As shown in Figure 14, we calculated a daily mean value of the cosmic ray intensity observed by high-energy neutron monitors (HNMs). In order to do that, we used data of five neutron monitors with geomagnetic cutoff rigidity ($R_c$) higher than 6 GV: Alma-Ata B ($R_c = 6.69$ GV), Athens ($R_c = 8.53$ GV), Mexico City ($R_c = 8.28$ GV), Rome ($R_c = 6.27$ GV) and Tsumeb ($R_c = 9.21$ GV). If $\Delta I_{\mathrm{TPC}}$ calculated by Equation (1) using $\Delta I_T$ obtained by a chosen method presents a higher Pearson correlation coefficient with the high-energy neutron monitor data (RHNM), then the greatest removal of temperature effect is assumed to be achieved by this method.

Table 2 shows the values of NRMSD and RHNM obtained for each method, while Table 3 shows a comparison between the values found for each parameter. On the left side of this table, we show NRMSD compared to the results found for the MSS method. For example, in the KWT column, NRMSD found for the GRD method is of the order of 40.7% higher than that obtained for the MSS method. On the right side of the Table 3, the values of correlation coefficients between the muon intensity corrected by temperature and RHNM are compared to the correlation coefficients found using muon data

**Table 2**
Values of the NRMSD between the Observed Muon Intensity Seasonal Variation and That Expected Due to Each Method (on the Left Side) and the RHNM Correlation Coefficient between the Average Cosmic Ray Intensity Seen by the Higher Cutoff ($R_c > 6\ GV$) Neutron Monitors and Muon Data Corrected by Temperature Using Each Method (on the Right Side)

| Methods | NRMDS ∗ 1e4 | | | | | RHNM | | | | |
|---|---|---|---|---|---|---|---|---|---|---|
| | KWT | NGY | HBT | SMS | Mean | KWT | NGY | HBT | SMS | Mean |
| Nothing | | | | | | 0.438 | 0.429 | 0.579 | 0.596 | 0.510 |
| ATE | 574 | 552 | 990 | 1351 | 866 | 0.730 | 0.802 | 0.815 | 0.752 | 0.775 |
| GRD | 620 | 529 | 1067 | 1305 | 880 | 0.746 | 0.746 | 0.810 | 0.732 | 0.759 |
| MMP | 1845 | 1637 | 2064 | 1443 | 1747 | 0.501 | 0.451 | 0.680 | 0.716 | 0.587 |
| ATE+MMP | 583 | 578 | 986 | **1247** | 848 | 0.734 | 0.808 | 0.828 | 0.775 | 0.786 |
| GRD+MMP | 572 | 555 | 1098 | 1252 | 869 | 0.766 | 0.765 | 0.813 | 0.766 | 0.777 |
| THR | 461 | 551 | 1485 | 1871 | 1092 | 0.789 | 0.761 | 0.848 | 0.759 | 0.789 |
| THR-L | **440** | 462 | **967** | 1371 | 810 | 0.831 | 0.842 | 0.876 | 0.779 | 0.832 |
| MSS | 441 | **459** | 971 | 1358 | **807** | **0.834** | **0.850** | **0.878** | **0.783** | **0.836** |
| EFF | 1142 | 2111 | 2224 | 2342 | 1955 | 0.566 | 0.475 | 0.583 | 0.595 | 0.555 |
| EFF-M | 580 | 569 | 1024 | 1392 | 891 | 0.762 | 0.789 | 0.854 | 0.757 | 0.790 |

**Note.** The lowest values of NRMSD and the highest values of RHNM are shown in underlined and bold. For better visualization, the values of NRMSD are shown multiplied by 1e4.

**Table 3**
Comparison between NRMSD and RHNM Found for Each Method

| Methods | Difference with Minimum NRMDS (%) | | | | | RHNM compared to uncorrected data (%) | | | | |
|---|---|---|---|---|---|---|---|---|---|---|
| | KWT | NGY | HBT | SMS | All | KWT | NGY | HBT | SMS | All |
| Nothing | | | | | | 0 (0.438) | 0 (0.429) | 0 (0.579) | 0 (0.596) | 0 (0.510) |
| ATE | +30.1 | +20.1 | +1.9 | +0.5 | +7.3 | +66.8 | +87.1 | +40.7 | +26.2 | +51.8 |
| GRD | +40.7 | +15.2 | +9.9 | −3.9 | +9.0 | +70.5 | +74.1 | +39.9 | +22.9 | +48.7 |
| MMP | +318.6 | +256.7 | +112.6 | +6.2 | +116.4 | +14.5 | +5.1 | +17.5 | +20.2 | +15.0 |
| ATE+MMP | +32.2 | +25.9 | +1.6 | **−8.2** | +5.1 | +67.8 | +88.5 | +43.0 | +30.0 | +54.1 |
| GRD+MMP | +29.8 | +20.8 | +13.1 | −7.9 | +7.7 | +75.1 | +78.4 | +40.4 | +28.4 | +52.3 |
| THR | +4.5 | +20.0 | +53.0 | +37.7 | +35.2 | +80.3 | +77.4 | +46.5 | +27.4 | +54.7 |
| THR-L | **−0.3** | +0.6 | **−0.4** | +0.9 | +0.3 | +89.9 | +96.4 | +51.3 | +30.7 | +63.0 |
| MSS | 0.0 (0.0441) | **0.0** (**0.0459**) | 0.0 (0.0971) | 0.0 (0.1358) | **0.0** (**0.0807**) | **+90.5** | **+98.3** | **+51.6** | **+31.4** | **+63.9** |
| EFF | +159.1 | +359.8 | +129.1 | +72.4 | +142.1 | +29.3 | +10.8 | +0.7 | −0.2 | +8.7 |
| EFF-M | +31.6 | +23.9 | +5.5 | +2.5 | +10.4 | +74.1 | +83.9 | +47.5 | +27.1 | +54.9 |

**Note.** On the left side is shown the difference of the NRMSD found for each method with the one found for the MSS method. On the right side is shown the enhancement of the RHNM correlation coefficient between the average cosmic ray intensity seen by the higher cutoff ($R_c > 6\ GV$) neutron monitor and the muon data corrected by temperature using each method compared to RHNM obtained using muon data uncorrected by temperature. The value of NRMSD obtained for the MSS method in each column and RHNM obtained for uncorrected data are shown within parentheses. The columns called "all" show the results obtained considering all detectors together. The lowest values of NRMSD and the highest values of RHNM are shown in underlined and bold.

uncorrected by temperature. As another example, RHNM obtained using the NGY muon intensity corrected by temperature using the GRD method is of the order of 70% greater than RHNM found using NGY data corrected only by the pressure effect. The columns labeled "all" show the results of all detectors together, which are calculated through the average of the values of NRMSD and RHNM coefficients obtained by each detector. We did not use the percentage values shown for calculating these averages. For example, the mean value of NRMSD found for the GRD method is 0.0880, which is about 9% greater than the average NRMSD of the MSS method which is equal to 0.0807. In a similar way, the average RHNM found for the GRD method is 0.758, which is 48.7% greater than 0.510 (the average value of RHNM obtained using muon data uncorrected by the temperature effect).

As we can see in the left side of Tables 2 and 3, considering all detectors together, the muon intensity variation due to the temperature effect calculated by the MSS method presents the smallest discrepancy with seasonal variation observed on the measured data. Similar values are obtained using the THR-L method. On the other hand, NRMSD found for the THR method tends to be about 35% higher. Considering the detectors individually, the results are a little different. The THR-L and MSS methods still present similar results, but they do not present the smallest value of NRMSD for SMS. In addition, the discrepancy between NRMSD found for the THR and THR-L methods is not so great for KWT.

Looking at the left side of these tables, we can also see a larger value of NRMSD obtained using the EFF and MMP methods. The MMP method only takes into account temperatures observed at the altitude of maximum muon production by

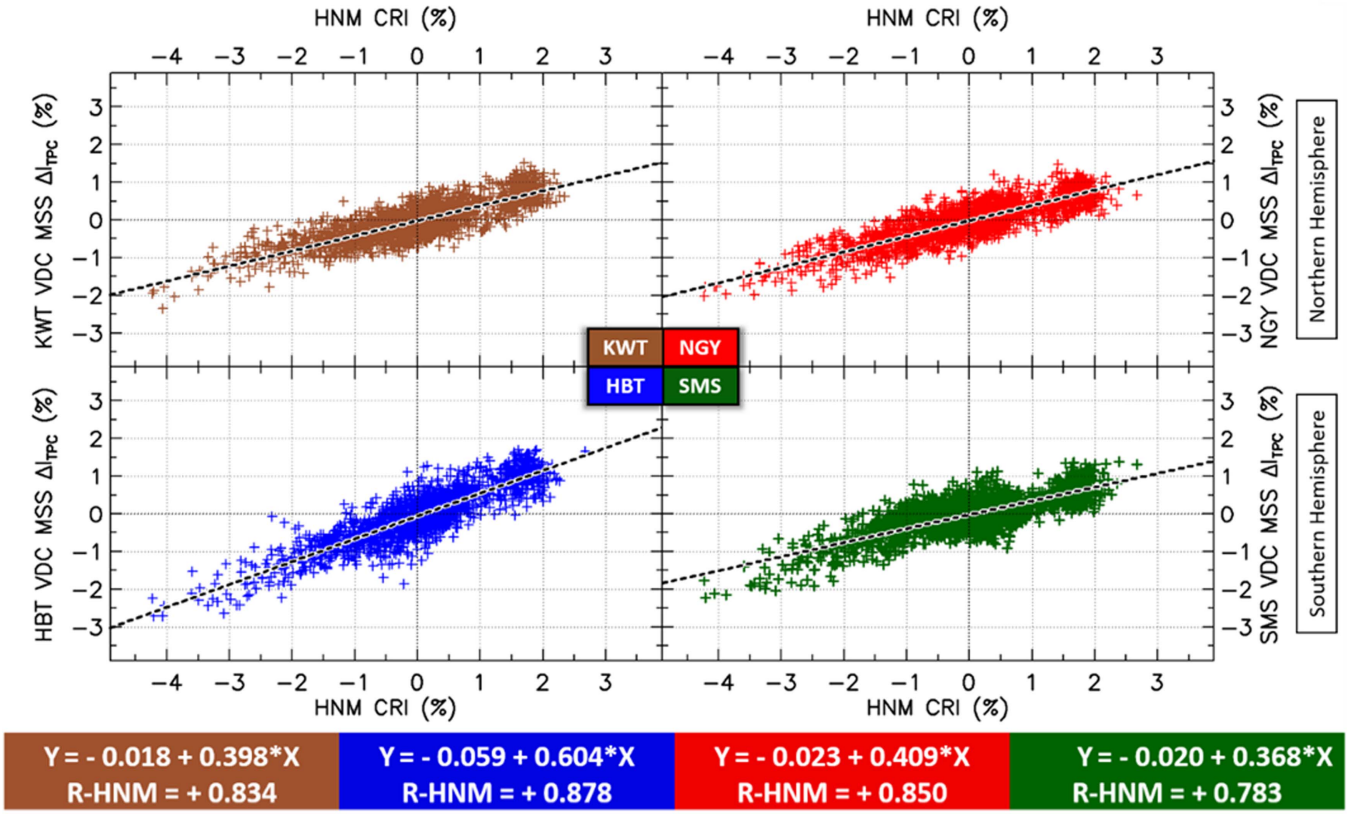


**Figure 15.** Linear correlation between the daily average of high-energy neutron monitor cosmic ray intensity variation (HNM CRI) and the pressure corrected muon intensity variation after removing temperature effect through the MSS method (MSS $\Delta I_{TPC}$) observed by the VDC of the KWT, NGY, HBT, and SMS detectors. The linear relation and the Pearson correlation coefficient (RHNM) between both are shown in the bottom.

pion decay, while the EFF method takes into account temperatures observed at altitudes higher than that. In both cases, NRMSD decreases considerably when we used modifications of these methods that take into account temperatures observed below the altitude of the MMP. Considering all detectors together, the NRMSD values for the EFF and MMP methods, which are more than 100% higher than the value obtained through the MSS method, change to values close to 10% when we used the EFF-M and GRD+MMP methods.

Looking at the right side of the Tables 2 and 3, we can first see that the muon intensity variation only corrected by pressure ($\Delta I_{PC}$) presents a higher correlation with the cosmic ray intensity variation recorded by high-energy neutron monitors for the detectors located in the southern hemisphere. While the RHNM of muon data uncorrected by temperature is approximately equal to 0.6 in the southern hemisphere, it is about 0.4 in the northern hemisphere. This is probably due to the lower seasonal variation amplitude of muon data measured by HBT and SMS (both in the southern hemisphere). Related to this north–south difference we can see that, in most cases, the enhancement of RHNM tends to be higher for KWT and NGY than for HBT and SMS. This does not occur only for the MMP method, where SMS presents a bigger increase of RHNM than that presented by the other detectors.

We can also see that the EFF method does not produce a significant improvement of RHNM when applied to data recorded by detectors located in the southern hemisphere. On the other hand, the increase of RHNM obtained using muon data corrected by temperature through the EFF-M method is significant and very close to the maximum values obtained in this analysis. Considering all detectors together, this method provides an enhancement of the order of 55% in the correlation between muon and neutron data, which without temperature correction was equal to 0.51. This increase is practically the same found using the THR Method. In turn, the changes that take into account local differences on this method (THR-L) enabled a better correlation of muon detectors with neutron monitor data. As expected, the THR-L and MSS methods present very similar enhancements of RHNM due to the resemblance between both methods already discussed above.

As occurs in the case of the EFF and EFF-M methods, the muon data corrected through the MMP method, which only considers the positive temperature effect, show significantly lower values of RHNM compared to the methods that also consider the negative effect. The enhancement in the correlation coefficient between muon and high-energy neutron data is three times larger when using the ATE+MMP or GDR+MMP methods. On the other hand, we cannot see major differences in the results of these combination methods in comparison with those that only consider the negative temperature effect. We obtain a significant increase on values of RHNM using only close to ground temperatures (GRD method) or using the altitude variation of the 100 hPa atmospheric isobar (ATE method) for removing the temperature effect on the muon data. The difference in the enhancement of RHNM obtained using these methods with that obtained using the THR Method is smaller than the difference found comparing the latter with the MSS method. While the obtained value of RHNM considering

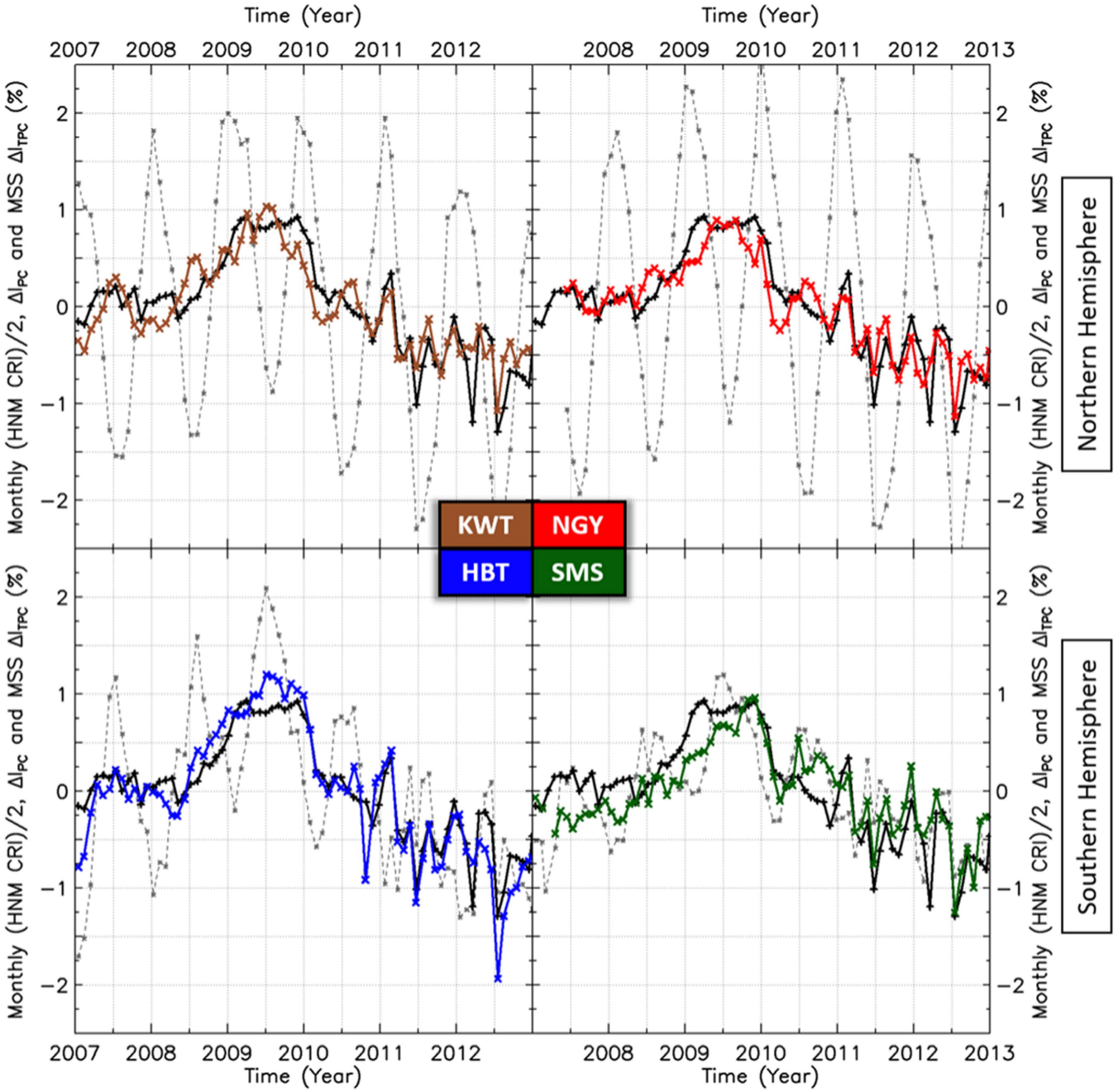


**Figure 16.** Monthly average of neutron monitor data together with muon data corrected and uncorrected by temperature. The dashed gray curves show the pressure corrected muon intensity variation ($\Delta I_{\rm PC}$) observed by the KWT, NGY, HBT, and SMS detectors, while the continuous colored curves show the pressure corrected muon intensity variation after removing the temperature effect through the MSS method (MSS $\Delta I_{\rm TPC}$). The continuous black curves show the average high-energy neutron monitor cosmic ray intensity variation (HNM CRI) divided by 2.

all detectors together is about 0.76 and 0.78 through the GRD and ATE methods respectively, it is close to 0.79 and 0.84 through the THR and MSS methods.

In comparison to all methods analyzed in this work, the 3 month running average of the muon variation expected due to temperature effect ($\langle \Delta I_T \rangle$) calculated by the MSS Method presents the smallest discrepancy with seasonal variation of the 3 month running average of the observed muon intensity variation corrected by pressure ($\langle \Delta I_{\rm PC}^{\rm SRT} \rangle$). In addition, daily values of muon data corrected by this method show the highest Pearson correlation coefficient with the average cosmic ray intensity seen by neutron monitors with geomagnetic cutoff rigidity higher than 6 GV.

Figure 15 shows the correlation between daily pressure corrected muon intensity variation after removing the temperature effect using the MSS method (MSS $\Delta I_{\rm TPC}$) and average high-energy neutron monitor cosmic ray intensity variation (HNM CRI) found for each detector. In this figure, we can also see the linear relation and the Pearson correlation coefficient (RHNM) between both. Although in this work we are interested only in the correlation coefficient, we notice that the relation between MSS $\Delta I_{\rm TPC}$ and HNM CRI found for

HBT is of the order of 50% higher than that found for the other detectors. This is related to the fact that the geomagnetic cutoff rigidities for NGY, KWT and SMS are around 10 GV, while for HBT it is of the order of 2 GV. Another possibility is the influence of the time variance of the mass weighted temperature coefficient. A more detailed analysis of the relation between the pressure and temperature corrected muon data recorded by the GMDN and neutron monitor data will be done in a future analysis. Figure 16 shows a comparison between the monthly intensity variation of muon data corrected by temperature using the MSS method and the monthly cosmic ray intensity variation observed by the neutron monitors from 2007 January up to 2012 December.

## 6. SUMMARY AND CONCLUSIONS

The analysis of cosmic ray intensity variation seen by muon detectors at Earth's surface can help us to understand astrophysical, solar, interplanetary and geomagnetic phenomena. However, before comparing cosmic ray intensity variations to extraterrestrial phenomena, it is necessary to take into account atmospheric effects. Among them, we can highlight the temperature effect, which produces a seasonal variation on the cosmic ray intensity observed by muon detectors. Usually, it is observed as a sinusoidal variation with maximum during winter related to the atmospheric expansion process (negative effect) and related to the temperature influence on pion decay (positive effect). In this work, we analyzed the temperature effect on the GMDN, which is composed of four ground detectors, two in the northern hemisphere and two in the southern hemisphere.

We noticed that the seasonal variation of temperatures observed near the altitude of MMP (assumed to be 16.5 km in this work) is in antiphase with the seasonal variation of temperatures observed near the surface for all four GMDN observation sites. The ground temperature is higher than its average value during summer, while temperatures near 16.5 km are lower than the average in the same period. This antiphase seasonal variation is also observed by looking at the atmospheric temperature arranged into isobars (not altitude) layers. Considering the seasonal variation of the ground and 16.5 km temperature, we can expect a ground muon intensity decrease during summer related to both (negative and positive) temperature effects: (I) the atmospheric expansion occurring due to the increase of close to ground temperatures; and (II) the reduction of the pion decay probability at the altitude of MMP associated with the temperature decrease in this altitude range. However, studies of the average tropopause temperature (i.e., the average temperature in the atmospheric region close to the altitude of MMP) show that this situation is not valid for high-latitude regions. In this latitude range, the ground and tropopause temperature seasonal variations tend to be in phase. The way this latitudinal dependence changes the influence of the temperature effect on muon detectors located at low, medium and high latitude should be investigated in future work.

We analyzed the muon intensity expected due to the temperature effect through seven methods together with some variations and combinations of them. We studied: (I) the Atmospheric Expansion (ATE) method which takes into account altitude variations of the isobar line where the MMP by pion decay is observed; (II) the Ground (GRD) method which only considers temperature changes observed near the ground; (III) the MMP method which only considers temperature changes observed at the altitude of MMP by pion decay; (IV) the ATE+MMP and GRD+MMP methods which combine the previous methods that only consider the negative effect with those that only consider the positive effect; (V) the Theoretical (THR) or Integral method which considers the muon production and decay theory for calculating the temperature effect, and its variation (THR-L method), which includes a local dependency neglected in the original method; (VI) the Mass Weighted (MSS) method which considers temperature variation along all the atmosphere through a unique parameter based in the atmospheric temperature weighted by the atmospheric depth; (VII) the Effective Temperature (EFF) method and the Modified Effective Temperature (EFF-M) method, where the first is generally used on analysis of underground muon detectors while the second is a modification of the first used for improving its results on ground muon detectors.

In general, we found a higher temperature influence on GMDN detectors located in the northern hemisphere than those located in the southern hemisphere. In other words, the same temperature deviation produces a higher muon intensity variation on the Kuwait and Nagoya detectors than that observed on the Hobart and São Martinho da Serra detectors. The temperature coefficients obtained using the GRD, ATE and MSS Methods are on average 1.3–1.6 times higher for the northern detectors. For the MMP method, it is three times larger. Comparing the seasonal variation observed on measured data and the muon intensity variation calculated by the THR method (which considers an equal influence of temperature on all detectors), we can see that this method over-reproduces the temperature effect on the southern detectors. Supposing that the temperature effect is the same for all detectors, we need to consider the existence of a local phenomenon (not related to temperature or pressure) more prominent in the southern hemisphere. This north–south difference in the temperature effect calculated by empirical methods cannot be related to the influence of temperature on detector electronics, since Kuwait, Nagoya (both in the northern hemisphere) and São Martinho da Serra (in the southern hemisphere) operate under a practically constant interior temperature. In addition, this difference probably cannot be related to pressure effect since, as we can see in Mendonça et al. (2013) and also in the Appendix, the barometric coefficients for Kuwait, Nagoya and São Martinho da Serra are the same (about $-0.12\%/\mathrm{hPa}$). Only Hobart, which has a lower geomagnetic cutoff rigidity than those other GMDN detectors, presents a higher barometric coefficient (about $-0.17\%/\mathrm{hPa}$).

Comparing the results obtained by the THR, THR-L and MSS methods, we noticed that by multiplying the local coefficient calculated on the THR-L method with the total temperature coefficient of the THR method, we found values very similar to the temperature coefficients found in the MSS method. Thus, we may understand the MSS method as the THR method influenced by local differences.

The EFF method, which is used for reproducing the temperature effect on underground muon detectors and mainly

considers temperature changes observed at altitudes higher than 30 km, did not present good results for three of the four ground detectors of the GMDN. In particular, it did not reproduce a clear seasonal variation for the Sao Martinho da Serra detector. The correlation between the compilation of temperature observed at highest altitude and the muon intensity variation observed by each detector is very different and tends to be higher in the northern hemisphere. The correlation is at least reasonable ($|R| > 0.5$) for Kuwait and Nagoya, but it is poor ($|R| < 0.3$) for Hobart and São Martinho da Serra. These results were greatly improved after we changed this method to consider temperature variation observed at altitudes between 5 and 16.5 km. In this case, the correlation changed to approximately 0.9 for the detectors located in the northern hemisphere detectors and at least to 0.6 for the southern hemisphere detectors. In the same way, the higher discrepancy between the muon intensity variation due to the temperature effect calculated by the EFF method and the seasonal variation observed in the measured data drastically reduced when we changed this method to take into account lower altitudes. Similar behavior was observed with the MMP method (which considers temperature changes at 16.5 km) and its combination with the GRD Method. As expected, the seasonal variation of the muon intensity observed at the ground by the GMDN detectors tends to be more related to temperature changes observed at low altitudes (below the altitude of MMP by pion decay).

The MSS method, in comparison to all methods analyzed in this work, was the one that presented the smallest discrepancy between the calculated and observed seasonal variation of the muon intensity related to the temperature effect. Furthermore, this variation gave the best results when compared to the neutron monitor data. We can therefore conclude that this method is shown to best remove the temperature effect on ground muon detectors.

The correlation between the muon intensity variation only corrected by pressure and the average cosmic ray intensity observed by high-energy neutron monitors, which was ∼0.59 for southern and ∼0.43 for northern detectors, increased to ∼0.84 after we corrected the data for temperature effect through the MSS method. Using the THR method, we found a correlation of the order of 0.79, which is close to the correlation found in those methods that only consider the temperature changes observed at ground (∼0.76) or that only consider the altitude variation of the 100 hPa isobar (∼0.77). Moreover, the muon intensity variation due to the temperature effect calculated by these two methods better reproduces the seasonal variation present in the uncorrected data than that calculated by the THR method. Including local differences in this method, i.e., using THR-L, the correlation between muon and neutron data changed to ∼0.83.

In summary, we analyzed several methods to correct by the temperature effect the cosmic ray data observed by muon detectors using the GMDN data. The best method was found to be the Mass Weighted Method, which considers the temperature along the entire atmosphere through weight function based on the air density. This method will be applied to GMDN data to perform space weather studies in the future.

The observations with the GMDN are supported in part by the joint research programs of the Institute for Space-Earth Environmental Research (ISEE), Nagoya University and the Institute for Cosmic Ray Research (ICRR) of the University of Tokyo. The observations are supported by Nagoya University with the Nagoya muon detector, by INPE, and UFSM with the São Martinho da Serra muon detector, and by the Australian Antarctic Division with the Hobart muon detector. The Kuwait muon detector is supported by the project SP01/09 of the Research Administration of Kuwait University. Neutron monitors of the Bartol Research Institute are supported by the National Science Foundation grant ATM-0000315. RRSdM acknowledges the São Paulo Research Foundation (FAPESP) for grants #2012/20594-0 and #2013/03530-0. CRB acknowledges the São Paulo Research Foundation (FAPESP) for grant #2014/24711-6. ADL acknowledges CNPq for grant 304209/2014-7. E.E. acknowledges CNPq for grant 302583/2015-7.

We also would like to thank Luiz Fermino Flores do Nascimento for helping us to solving unexpected problems on the SMS observatory power supply and internet connection. We thank the Global System Divisions (GDS) of the National Oceanic and Atmospheric Administration Earth System Research Laboratory (NOAA/ESRL) for processing and distributing radiosonde (low-altitude atmospheric temperature) data used in this work; and the SABER instrument team and GATS Inc. for processing and distributing the high-altitude atmospheric temperature data used in this work.

## APPENDIX
## ATMOSPHERIC PRESSURE (BAROMETRIC) EFFECT ANALISYS AND CORRECTION

As mentioned in the introduction, the principal and best known atmospheric effect on the secondary cosmic ray intensity observed at ground is the barometric (or pressure) effect. Put simply, when a secondary particle is moving toward the surface its probability to interact with the atmosphere increases as it approaches the ground, due to the higher air density at low altitudes. Thus, the secondary cosmic ray intensity at a given altitude tends to change according to the amount of air mass above this altitude. When an atmospheric structure changes the total air mass at ground, which can be characterized by an atmospheric pressure decrease, we observe a secondary cosmic ray intensity increase. Figure 17 shows an example of this kind of event observed during the passage of the Typhoon Melor above the Nagoya detector region in 2009 October. In a more complex overview of the pressure effect on secondary cosmic rays muons, we need also to take into account its influence on muon decay and generation processes (Sagisaka 1986).

There are different ways to approach experimentally the pressure influence on secondary cosmic ray intensity observed at ground. The two most common describe the cosmic ray intensity variation associated with the barometric effect through a linear (e.g., Trefall 1955b; Zazyan et al. 2015) or an exponential (e.g., Lindgren 1962; Maghrabi et al. 2012) dependence with the pressure deviation. In both cases, the magnitude of the pressure influence is given by a coefficient (the barometric coefficient). In this work, we considered the following expression to describe the pressure influence on the muon intensity observed at ground:

$$I_P = I_0 * e^{0.01*\beta*(P-P_0)} \quad (17)$$

where $I_P$ is the muon count rate expected when the atmospheric pressure (in hPa) is equal to $P$ considering an initial count rate

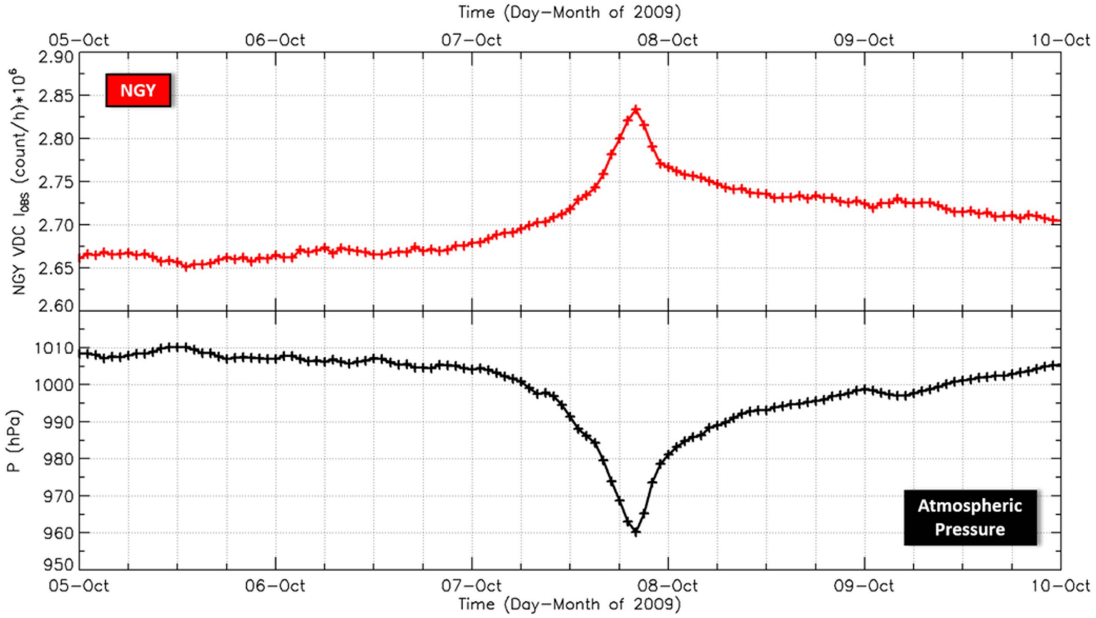


**Figure 17.** Secondary cosmic ray count rate and atmospheric pressure variation observed by the NGY detector during the passage of Typhoon Melor in 2009. The red line shows the NGY vertical directional channel muon count rate ($I_{OBS}$), while the black line shows the measured atmospheric pressure above this detector in the period between 2009 October 5 and 2009 October 10.

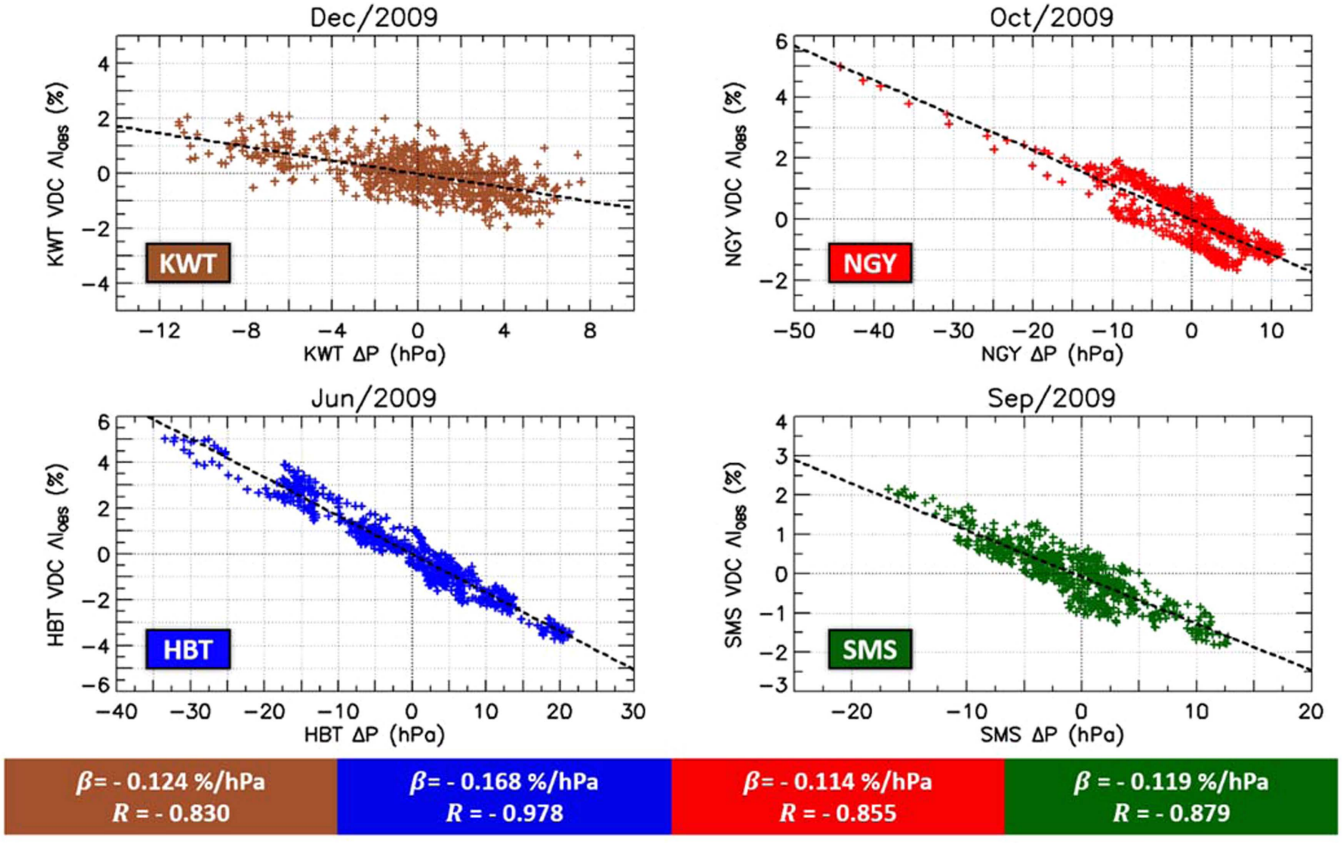


**Figure 18.** Linear correlation between the atmospheric pressure deviation ($\Delta P$) and the logarithmic variation of the muon count rate ($\Lambda I_{OBS}$) observed by the VDC of the KWT, NGY, HBT, and SMS detectors. The barometric coefficient ($\beta$) and the Pearson correlation coefficient ($R$) obtained on each linear correlation are shown in the lower panel.

($I_0$) observed when the atmospheric pressure is equal to a chosen value $P_0$. In this equation, $\beta$ is the barometric coefficient given in %/hPa. When this coefficient is theoretically calculated, its value depends, among other parameters, on the differential energy spectrum of secondary muons (Sagisaka 1986). In this work, it was empirically

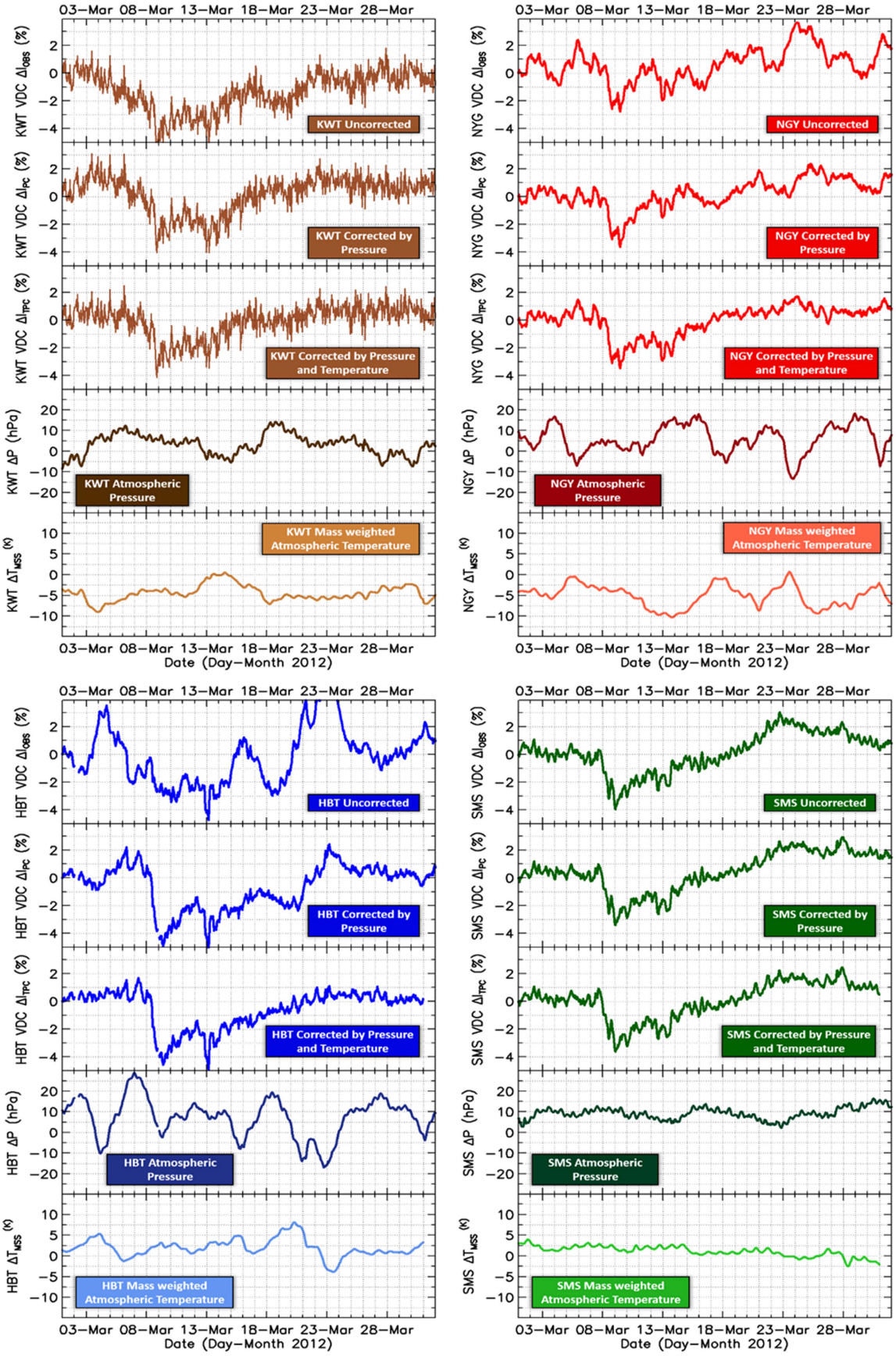


**Figure 19.** Uncorrected ($\Delta I_{OBS}$), only pressure corrected ($\Delta I_{PC}$) and pressure and temperature corrected ($\Delta I_{TPC}$) muon intensity variations observed by the new correlation system VDC of the KWT, NGY, HBT, and SMS detectors on 2012 March. The bottom two panels for each detector show variations of the atmospheric pressure deviation ($\Delta P$) and the mass weighted atmospheric temperature ($\Delta T_{MSS}$) observed in this period.

obtained by rearranging Equation (17) as follows:

$$\Lambda I(t) = ln\left[\frac{I_{OBS}(t)}{I_M}\right] * 100 = \beta^{*}\Delta P(t) \quad (18)$$

$$\Delta P(t) = P(t) - P_M \quad (19)$$

where $\Lambda I(t)$ is the natural logarithmic variation of the muon count rate observed at time $t$, i.e., $I_{OBS}(t)$, in relation to an average muon count rate $I_M$; $P(t)$ is the atmospheric pressure measured at ground at time $t$; and $P_M$ is the mean value of $P(t)$ in the same period that was used to calculated $I_M$.

In order to empirically obtain the barometric coefficient ($\beta$) through a linear regression between $\Lambda I(t)$ and $\Delta P$, we need to choose a period when the muon intensity variation is predominantly influenced by a significant pressure variation. If we choose a period when the influence of effects related to solar, interplanetary or other atmospheric phenomena is higher than that related to the atmospheric pressure, we cannot calculate an accurate value for $\beta$. Following this concept, we chose a short period (one month) to avoid long-timescale effects such as those related to the 11 year solar cycle and seasonal temperature changes. For each detector, we used the month of 2009 (i.e., during the solar minimum) in which we found the highest correlation between $\Lambda I(t)$ and $\Delta P$. For the NGY detector, the highest correlation was found in October (the same month that Typhoon Melor hit Japan). The months of June, September and December were chosen for the HBT, KWT and SMS detectors, respectively. The correlation and barometric coefficients found for the VDC of each detector in these periods are shown in Figure 18. It is possible to see in this figure a good correlation ($R > 0.80$) between the logarithmic variation of the muon count rate and the atmospheric pressure deviation for all detectors. In this figure, it is also possible to see a higher value of $R$ for the HBT detector in comparison with other three. In a similar way, the barometric coefficient found for this detector is a little higher than that found for the others. While $\beta$ is about $-0.17\%$/hPa for HBT, it is about $-0.12\%$/hPa for KWT, NGY and SMS. A possible reason for this difference is the small geomagnetic cutoff rigidity at the HBT region, which is about ten times lower than that found for the other detectors (see Section 2). The total muon intensity observed at HBT, therefore, may be more influenced by low-energy muons, which are more susceptible to the barometric effect (see Figure 3 of Allkofer et al. 1975 or Figure 1 of Cecchini & Sioli (2000) for more details about the differences on the sea-level muon spectra related to geomagnetic cutoff rigidity change).

Considering the cosmic ray count corrected by the pressure ($I_{CP}$) is that which would be observed when the atmospheric pressure is equal to its mean value ($P_M$), it is possible to write Equation (17) as:

$$I_{PC}(t) = I_{OBS}(t) * e^{0.01*\beta*[P_M - P(t)]} \quad (20)$$

$$I_{PC}(t) = I_{OBS}(t) * e^{-0.01*\beta*[P(t) - P_M]} \quad (21)$$

$$I_{PC}(t) = I_{OBS}(t) * e^{-0.01*\beta*\Delta P(t)} \quad (22)$$

where $I_{OBS}(t)$ is the observed muon count rate at time $t$, $\Delta P(t)$ is the deviation of the atmospheric pressure obtained at the same time $t$ and $\beta$ is the barometric coefficient, which has a negative value and is given in %/hPa.

Using Equation (23), we removed the barometric effect from the muon count rates observed by the new correlation system VDC of the HBT, KWT, NGY, and SMS detectors between 2007 and 2012. After this, we calculated the muon intensity variation corrected by the pressure effect ($\Delta I_{PC}$), whose daily mean values were used in the temperature effect analysis, as follows:

$$\Delta I_{PC}(t) = \frac{I_{PC}(t) - \langle I_{PC}\rangle}{\langle I_{PC}\rangle} * 100 \quad (23)$$

where $\langle I_{PC}\rangle$ is the average muon count rate corrected by pressure effect between 2007 and 2012.

Figure 19 shows an example of the temporal variations of the muon intensity uncorrected ($\Delta I_{OBS}$), corrected only by pressure ($\Delta I_{PC}$) and corrected by both pressure and temperature effects ($\Delta I_{TPC}$) observed in 2012 March. During the period shown in this figure, a great Forbush decrease was observed in many cosmic ray detectors around the world. The Forbush decrease is known as a cosmic ray intensity reduction associated with the passage of interplanetary structures in Earth's vicinity. The classical behavior of the cosmic ray intensity during a Forbush decrease, and more information about it, can be found in Cane (2000). In general, the cosmic ray intensity shows a very fast decrease accompanied by a slow recovery phase in these events. As we can see in Figure 19, these classical characteristics are hard to see in the uncorrected HBT and NGY data. After the pressure correction, the first step (fast decrease) becomes visible in all detector data, but the recovery phase in the HBT data appears significantly different from that present on the other detectors' data. In a less evident way, the recovery phase observed in the NGY data also appears to be different from that observed in the KWT and SMS data, which are more similar to what is expected in a classical Forbush decrease. After the muon intensity was corrected by temperature (using the MSS method), the classical features of the Forbush decrease became visible in all detector data. A clear Forbush decrease can be observed even in the KWT detector data, which have a larger statistical error due to its lower count rate.

## REFERENCES


Allkofer, O. C., Clausen, K., & Dau, W. D. 1975, NCimL, 12, 107
Ambrosio, M., Antolinis, R., Auriemma, G., et al. 1997, APh, 7, 109
Barrett, P. H., Bollinger, L. M., Cocconi, G., et al. 1952, RvMP, 24, 133
Berkova, M. D., Belova, A. V., Eroshenko, E. A., & Yanke, V. G. 2011, BRASP, 75, 820
Bieber, J. W., Eroshenko, E., Evenson, P. et al. (ed.) 2009, Cosmic Rays and Earth (Dordrecht: Springer)
Blackett, P. M. S. 1938, PhRvL, 54, 973
Cane, H. V. 2000, SSRv, 93, 55
Cecchini, S., & Sioli, M. 2000, arXiv:hep-ex/0002052
De Mendonça, R. R. S., Raulin, J.-P., Echer, E., et al. 2013, JGRA, 118, 1403
Dorman, L. 2004, Cosmic Rays in the Earth's Atmosphere and Underground (Dordrecht: Kluwer)
Dorman, L. 2009, Cosmic Rays in Magnetospheres of the Earth and other Planets (New York: Springer)
Duperier, A. 1949, PPSA, 62, 684
Duperier, A. 1951, JATP, 1, 296
French, W. R., Jr., & Chasson, R. L. 1959, JATP, 14, 1
Fushishita, A., Kuwabara, T., Kato, C., et al. 2010, ApJ, 715, 1239
Gille, J. C., & House, F. B. 1971, JAtS, 28, 1427
Grieder, P. K. F. 2001, Cosmic Rays at Earth (Amsterdam: Elsevier)
Harman, C. V., & Hatton, C. J. 1968, CaJPh, 46, S1052
Heber, B., & Kota, J. (ed.) 2014, Cosmic Rays in the Heliosphere (New York: Springer)
Hess, V. F. 1940, PhRvL, 57, 781
Kudela, K., Storini, M., Hofer, M. Y., & Belov, A. 2000, SSRv, 93, 153
Kuwabara, T., Bieber, J. W., Clem, J., et al. 2006, SpWea, 4, S08001
Kuwabara, T., Bieber, J. W., Evenson, P., et al. 2009, JGR, 114, A05109
Lindgren, S. 1962, Tell, 14, 44
Liu, Y., Taoling, X., & Jun, L. 2014, AdSpR, 54, 2274

Maghrabi, A. H., Al Harbi, H., Al-Mostafa, Z. A., et al. 2012, AdSpR, 50, 700
Mendonça, R. R. S., Echer, E., Dal Lago, A., et al. 2013, in Proc. ICRC 33, Solar and Heliospheric Physics, ed. R. C. Shellard, 0385
Miroshnichenko, L. 2001, Solar Cosmic Rays (Dordrecht: Kluwer)
Mlynczak, M. G., Martin, G., Marshall, B. T., et al. 2007, JGR, 112, 306
Munakata, K., Kuwabara, T., Bieber, J. W., et al. 2005, AdSpR, 35, 2357
Murakami, K., Nagashima, K., Sagisaka, S., et al. 1979, NCimC, 2, 635
Okazaki, Y., Fushishita, T., Narumi, T., et al. 2008, ApJ, 681, 693
Rockenbach, M., Dal Lago, A., Schuch, N. J., et al. 2014, SSRv, 182, 1
Sagisaka, S. 1986, NCimC, 9, 809
Tilav, S., Desiati, P., Kuwabara, T., et al. 2009, in Proc. ICRC, 31, 1398
Trefall, H. 1955a, PPSA, 68, 893
Trefall, H. 1955b, PPSA, 68, 953
Yanchukovsky, V. L., Filimonov, G. Y., & Hisamov, R. Z. 2007, BRASP, 71, 1038
Yasue, S., Munakata, K., & Kato, C. 2003, in Proc. ICRC 28, Frontier Science Series, ed. T. Kajita (Tokyo: Universal Academy Press), 3461
Zazyan, M., Ganeva, G., Berkova, M., et al. 2015, JSWSC, 5, A6